AD-A101 190 NAVAL SURFACE WEAPONS CENTER SILVER SPRING MD F/G 20/14
SPACE CHARGE WAVES IN A CYLINDRICAL WAVEGUIDE WITH ARBITRARY WA--ETC(U)
FEB 81 H S UHM
UNCLASSIFIED NSWC/TR-81-65 NL

1 OF 1
AD
A101 190

END
DATE
FILMED
7-81
DTIC

NSWC TR 81-65

LEVEL II

AD A101190

SPACE CHARGE WAVES IN A CYLINDRICAL WAVEGUIDE WITH ARBITRARY WALL IMPEDANCE

BY HAN S. UHM

RESEARCH AND TECHNOLOGY DEPARTMENT

20 FEBRUARY 1981

NAVAL SURFACE WEAPONS CENTER

Dahlgren, Virginia 22448 • Silver Spring, Maryland 20910

UNCLASSIFIED

SECURITY CLASSIFICATION OF THIS PAGE (When Data Entered)

REPORT DOCUMENTATION PAGE

READ INSTRUCTIONS BEFORE COMPLETING FORM

1. REPORT NUMBER: (14) NSWC/TR-81-65
2. GOVT ACCESSION NO.: AD-A104490
3. RECIPIENT'S CATALOG NUMBER

4. TITLE (and Subtitle): (6) SPACE CHARGE WAVES IN A CYLINDRICAL WAVEGUIDE WITH ARBITRARY WALL IMPEDANCE.

5. TYPE OF REPORT & PERIOD COVERED: (9) Final rept., December 1980

6. PERFORMING ORG. REPORT NUMBER

7. AUTHOR(s): (10) HAN S. UHM

8. CONTRACT OR GRANT NUMBER(s)

9. PERFORMING ORGANIZATION NAME AND ADDRESS

NAVAL SURFACE WEAPONS CENTER
WHITE OAK
SILVER SPRING, MARYLAND 20910

10. PROGRAM ELEMENT, PROJECT, TASK AREA & WORK UNIT NUMBERS: 0

11. CONTROLLING OFFICE NAME AND ADDRESS (11)

12. REPORT DATE: 20 Feb [redacted]81

13. NUMBER OF PAGES: 57 (12) 64

14. MONITORING AGENCY NAME & ADDRESS (if different from Controlling Office)

15. SECURITY CLASS. (of this report): UNCLASSIFIED

15a. DECLASSIFICATION/DOWNGRADING SCHEDULE

16. DISTRIBUTION STATEMENT (of this Report)

Approved for public release; distribution unlimited

17. DISTRIBUTION STATEMENT (of the abstract entered in Block 20, if different from Report)

18. SUPPLEMENTARY NOTES

19. KEY WORDS (Continue on reverse side if necessary and identify by block number)

Space Charge Wave
Electron Beam
Waveguide
Wall Impedance

20. ABSTRACT (Continue on reverse side if necessary and identify by block number)

Properties of the space charge waves in a solid relativistic electron beam propagating in a cylindrical waveguide is investigated, including the important influence of arbitrary wall impedance. The stability analysis is carried out within the framework of the linearized Vlasov-Maxwell equations. In order to examine the influence of the axial momentum spread on the stability behavior, it is assumed that all electrons have a Lorentzian distribution in the axial canonical momentum. One of the most important features of the analysis is that, for short axial wavelength perturbations, →

DD FORM 1473, 1 JAN 73 — EDITION OF 1 NOV 65 IS OBSOLETE

S/N 0102-014-6601

UNCLASSIFIED 421563

SECURITY CLASSIFICATION OF THIS PAGE (When Data Entered)

 Item 20 (continuted)

the eigenfunction can be described by a Bessel function. Moreover, the condition for zero phase velocity of the space charge wave is also obtained, in connection with collective ion acceleration. Space charge wave properties for a dielectric loaded waveguide are also investigated. For appropriate choice of dielectric constant ε and thickness of the dielectric material, it is shown that a strong mode coupling occurs, exhibiting the growth rate of instability comparable to the beam plasma frequency. The physical mechanism of instability is the Cherenkov radiation.

FOREWORD

Properties of the space charge waves in a solid relativistic electron beam propagating in a cylindrical waveguide is investigated, including the important influence of arbitrary wall impedance. The stability analysis is carried out within the framework of the linearized Vlasov-Maxwell equations. In order to examine the influence of the axial momentum spread on the stability behavior, it is assumed that all electrons have a Lorentzian distribution in the axial canonical momentum. One of the most important features of the analysis is that, for short axial wavelength perturbations, the eigenfunction can be described by a Bessel function. Moreover, the condition for zero phase velocity of the space charge wave is also obtained, in connection with collective ion acceleration. Space charge wave properties for a dielectric loaded waveguide are also investigated. For appropriate choice of dielectric constant ε and thickness of the dielectric material, it is shown that a strong mode coupling occurs, exhibiting the growth rate of instability comparable to the beam plasma frequency. The physical mechanism of instability is the Cherenkov radiation. This research was supported by the Independent Research Fund at the Naval Surface Weapons Center.

H. R. RIEDL
By direction

CONTENTS

ILLUSTRATIONS

ILLUSTRATIONS (CON'T)

ILLUSTRATIONS (CON'T)

I. INTRODUCTION

In recent years, there has been a growing interest in the space charge waves[1-4] in a relativistic electron beam, in connection with collective ion acceleration[3-6] and intense microwave generation.[7-10] For the most part, previous theoretical analyses[1-4] of the space charge waves are limited and incomplete. However, a complete analysis of the space charge wave is required to optimize the collective ion acceleration and microwave generation. In this regard, in the present article, we develop a unified theory of the space charge wave in a relativistic electron beam, including the important influence of an arbitrary wall impedance on the stability behavior.

Equilibrium and stability properties are calculated for the choice of electron distribution function [Eq. (3)]

$$f_b^0(H, P_\theta, P_z) = \frac{\hat{n}_b \Delta}{2\pi^2 \gamma_b m} \frac{\delta(H - \omega_b P_\theta - \hat{\gamma} mc^2)}{(P_z - \gamma_b m \beta_b c)^2 + \Delta^2} ,$$

where H is the energy, P_θ is the canonical angular momentum, P_z is the axial canonical momentum, and $\gamma_b = (1 - \beta_b^2)^{-1/2}$, $\hat{\gamma}$, $\hat{n}_b$, and Δ are constants. The stability analysis of the space charge wave is carried out within the framework of the linearized Vlasov-Maxwell equations, assuming that $\nu/\gamma_b \ll 1$, where ν is Budker's parameter. The formal dispersion relation (20) of the space charge wave for azimuthally symmetric electromagnetic perturbation ($\partial/\partial\theta = 0$) is obtained in Sec. II, including the important influence of finite wall impedance Z, which is generally an arbitrary function of the eigenfrequency ω and axial wavenumber k. Particularly, we emphasize that Eq. (20) is derived with no a priori assumption that the beam radius R_0 is much less than the wall radius R_w. In this regard, the dispersion relation in Eq. (20) can be used to investigate properties of the space charge wave for a broad range of system parameters.

In Sec. III, the resistive wall instability[10] with an arbitrary impedance is investigated in general, assuming that all electrons have the same value of axial canonical momentum ($\Delta = 0$). It is shown that an inductive impedance wall is most unstable. Particularly, the maximum growth rate of the general resistive wall instability occurs at the axial wavenumber k satisfying $2k^2R_0^2 = \gamma_b^2(\xi_i^2 - \xi_r^2)$, where the parameter $\xi = \xi_r + i\xi_i$ is the root of $\xi J_1(\xi)/J_0(\xi) = F$, $J_\ell(x)$ is the Bessel function of the first kind of order ℓ and F is the wave admittance at the beam surface [Eq. (19)].

Properties of the space charge wave in a perfectly conducting waveguide is investigated in Sec. IV, in connection with intense microwave generation[7-10] and collective ion acceleration.[3-6] It is found that the wave admittance F in a perfectly conducting waveguide is purely capacitive, thereby indicating a stable propagation of the space charge wave. However, for short axial wavelength perturbation satisfying $kR_0/\gamma_b \gtrsim 10$ [which is typical in the free electron laser application[7,8]], the electrostatic eigenfunction of the space charge wave can be accurately represented by a Bessel function. In the present experiments[4-6] of collective ion acceleration, the phase velocity of the space charge wave is initially required to be zero, in order to trap and accelerate ions. In this regard, in Sec. IV, we also obtain the condition for the phase velocity $\omega/k = 0$. That is [Eq. (42)],

$$\frac{4\nu}{\gamma_b} = (\gamma_b^2 - 1)(\xi_r^2 + k^2R_0^2).$$

We therefore find from Eq. (42) that the typical Budker's parameter for the zero phase velocity is order of unity in a practical range of physical parameters for collective ion acceleration.

Space charge wave properties for a dielectric loaded waveguide are investigated in Sec. V, assuming that the impedance of the dielectric material is purely reactive (i.e., the dielectric constant is perfectly real). In a range of physical parameters, it is shown that the phase velocity of the vacuum dielectric waveguide mode is less than the beam velocity, exhibiting possibilities of a Cherenkov radiation.[9,11] In fact, a strong mode coupling between the vacuum dielectric waveguide mode and the beam streaming mode occurs at the axial wavenumber satisfying $2k^2R_0^2 = \gamma_b^2(\xi_i^2 - \xi_r^2)$. We therefore conclude that the Cherenkov radiation in a dielectric loaded waveguide is a typical example of the inductive impedance (Sec. III). Several points are noteworthy in the analysis of Sec. V. First, the maximum growth rate of instability is order of the beam plasma frequency. In this regard, the Cherenkov radiation can be utilized to produce high power microwave. However, the growth rate of instability decreases substantially with increasing value of the axial momentum spread. Second, the wavelength of the microwave radiation generated by this instability can be less than a centimeter for a subcentimeter beam radius R_0. Finally, we note that the growth rate and bandwidth of instability increase rapidly as the surface of dielectric material approaches to the beam surface ($R_0/R_w \rightarrow 1$).

II. THEORETICAL MODEL

The equilibrium configuration consists of a relativistic electron beam column that is infinite in axial extent and aligned parallel to a uniform applied magnetic field $B_0\hat{e}_z$. The electron beam radius is denoted by R_0, and a finite-impedance wall is located at radius $r = R_w$. Cylindrical polar coordinates (r,θ,z) are introduced. Moreover, in the present analysis, we assume

$$\nu/\gamma_b << 1 , \qquad (1)$$

where $\nu = N_b e^2/mc^2$ is Budker's parameter,

$$N_b = 2\pi \int_0^{R_w} dr\; r\; n_b^0(r) ,$$

is the number of electrons per unit axial length, $n_b^0(r)$ is the equilibrium electron density, c is the speed of light in vacuo, -e and m are the electron charge and rest mass, respectively, and $\gamma_b mc^2$ is the characteristic electron energy in the laboratory frame. Consistent with the low-intensity assumption in Eq. (1), we also assume

$$\omega_{pb}^2/\omega_{cb}^2 << 1, \qquad (2)$$

where $\omega_{pb}^2 = 4\pi e^2 \hat{n}_b/\gamma_b m$ is the plasma frequency-squared and $\omega_{cb} = eB_0/\gamma_b mc$ is the electron cyclotron frequency.

In the present analysis, we investigate stability properties for the choice of equilibrium distribution function

$$f_b^0(H,P_\theta,P_z) = \frac{\hat{n}_b\Delta}{2\pi^2\gamma_b m}\,\frac{\delta(H - \omega_b P_\theta - \hat{\gamma}mc^2)}{(P_z - \gamma_b m\beta_b c)^2 + \Delta^2} , \qquad (3)$$

where $H = (m^2c^4 + c^2p^2)^{1/2} - e\phi_0(r)$ is the total energy, $P_\theta = r[p_\theta - (e/2c)rB_0]$ is the canonical angular momentum, $P_z = p_z - (e/c)A_z^s(r)$ is the axial canonical momentum, $\phi_0(r)$ and $A_z^s(r)$ are the equilibrium electrostatic and axial component of vector potentials, respectively, $\gamma_b = (1 - \beta_b^2)^{-1/2}$, $\hat{\gamma}$, $\hat{n}_b$, and Δ are constants.

In the subsequent perturbation analysis, use is made of the linearized Vlasov-Maxwell equations for azimuthally symmetric perturbations $(\partial/\partial\theta = 0)$ about a solid electron beam described by Eq. (3). We adopt a normal-mode approach in which all perturbations are assumed to vary according to

$$\delta\psi(\mathbf{x},t) = \hat{\psi}(r)\exp[i(kz - \omega t)] ,$$

where $\mathrm{Im}\omega > 0$. Here, ω is the complex eigenfrequency and k is the axial wavenumber. The Maxwell equations for the perturbed electric and magnetic field amplitudes can be expressed as

$$\begin{aligned} \nabla \times \hat{\mathbf{E}}(\mathbf{x}) &= i(\omega/c)\hat{\mathbf{B}}(\mathbf{x}) , \\ \nabla \times (1/\mu)\hat{\mathbf{B}}(\mathbf{x}) &= (4\pi/c)\hat{\mathbf{J}}(\mathbf{x}) - i(\omega/c)\epsilon\hat{\mathbf{E}}(\mathbf{x}) , \end{aligned} \tag{4}$$

where ϵ and μ are the dielectric constant and permeability, respectively, $\hat{\mathbf{E}}(\mathbf{x})$ and $\hat{\mathbf{B}}(\mathbf{x})$ are the perturbed electric and magnetic fields, and

$$\hat{\mathbf{J}}(\mathbf{x}) = -e\int d^3p\ \mathbf{v}\ \hat{f}_b(\mathbf{x},\mathbf{p}) , \tag{5}$$

is the perturbed current density. Note that $\epsilon = \mu = 1$ in vacuo. In Eq. (5),

$$\hat{f}_b(\mathbf{x},\mathbf{p}) = e\int_{-\infty}^{0} d\tau\ \exp(-i\omega\tau)\left(\hat{\mathbf{E}}(\mathbf{x}') + \frac{\mathbf{v}' \times \hat{\mathbf{B}}(\mathbf{x}')}{c}\right) \cdot \frac{\partial}{\partial \mathbf{p}'} f_b^0 , \tag{6}$$

is the perturbed distribution function, $\tau = t' - t$, and the particle trajectories $\mathbf{x}'(t')$ and $\mathbf{p}'(t')$ satisfy $d\mathbf{x}'/dt' = \mathbf{v}'$ and $d\mathbf{p}'/dt' = -e\mathbf{v}' \times \mathbf{B}_0^s/c$, with "initial" conditions $\mathbf{x}'(t' = t) = \mathbf{x}$ and $\mathbf{v}'(t' = t) = \mathbf{v}$.

In general, the permeability μ of a dielectric material even in the wall differs from unity by only a few parts in 10^5. Therefore, we approximate $\mu = 1$ in the remainder of this paper. Making use of Eq. (4), it is straightforward to show that

$$\hat{E}_r(r) = (kc/\omega\varepsilon)\hat{B}_\theta(r) ,$$

$$\hat{B}_\theta(r) = i[\omega\varepsilon/c(\omega^2\varepsilon/c^2 - k^2)][\partial\hat{E}_z(r)/\partial r] , \tag{7}$$

and

$$\left(\frac{1}{r}\frac{\partial}{\partial r} r \frac{\partial}{\partial r} + \frac{\omega^2}{c^2}\varepsilon - k^2\right)\hat{E}_z(r) = 4\pi ik\left[\hat{\rho}(r) - \frac{\omega}{c^2k}\hat{J}_z(r)\right] , \tag{8}$$

where $\hat{B}_\theta$ is the azimuthal component of the perturbed magnetic field, and $\hat{E}_r$ and $\hat{E}_z$ are the radial and axial components, respectively, of the perturbed electric field, $\hat{\rho}(r)$ is the perturbed charge density and $\hat{J}_z(r)$ is the axial component of the perturbed current density.

To lowest order, the axial motion of the particle orbit is free-streaming

$$z' = z + \frac{p_z}{\gamma m}(t' - t) . \tag{9}$$

Moreover, within the context of Eq. (2), we neglect the terms proportional to $\hat{\underset{\sim}{E}}_\perp(r)$ on the right-hand side of Eq. (6), where $\hat{\underset{\sim}{E}}_\perp(r)$ is the transverse component of the perturbed electric field. Finally we assume a slow rotational equilibrium characterized by

$$\omega_b \simeq \omega_b^- = \frac{\omega_{cb}}{2}\left[1 - \left(1 - \frac{2\omega_{pb}^2}{\gamma_b^2\omega_{cb}^2}\right)^{1/2}\right] , \tag{10}$$

thereby approximating[12]

$$r' \simeq r , \tag{11}$$

in the arguments of the perturbation amplitudes on the right-hand side of Eq. (6).

Substituting Eqs. (9) and (11) into Eq. (6), we obtain the perturbed distribution function

$$\hat{f}_b(r,\underset{\sim}{p}) = \frac{ei}{\omega - kp_z/\gamma m}\,\hat{E}_z(r)\,\frac{\partial f_b^0}{\partial p_z} . \tag{12}$$

Carrying out the momentum integration with Eqs. (3) and (12), the differential equation (8) can be expressed as

$$\begin{aligned} &\left(\frac{1}{r}\frac{\partial}{\partial r}\, r\,\frac{\partial}{\partial r} + T^2\right)\hat{E}_z(r) = 0 , \quad 0 \le r < R_0 , \\ &\left(\frac{1}{r}\frac{\partial}{\partial r}\, r\,\frac{\partial}{\partial r} + p^2\right)\hat{E}_z(r) = 0 , \quad R_0 < r < R_w , \end{aligned} \tag{13}$$

where

$$\begin{aligned} T^2 &= \left(k^2 - \frac{\omega^2}{c^2}\right)\left[\frac{\omega_{pb}^2}{\gamma_b^2(\omega - k\beta_b c + ik\Delta/\gamma_b^3 m)^2} - 1\right] , \\ p^2 &= \frac{\omega^2}{c^2} - k^2 , \end{aligned} \tag{14}$$

and the beam radius R_0 is defined by

$$R_0^2 = 2c^2(\hat{\gamma} - \gamma_b)/\gamma_b(\omega_b\omega_{cb} - \omega_b^2 - \omega_{pb}^2/2\gamma_b^2) . \tag{15}$$

For the convenience in the future analysis, we define the wave impedance $Z(\omega,k)$ of the wall as

$$Z(\omega,k) = -i(\omega R_w/c)\,\frac{\hat{E}_z(R_w)}{\hat{B}_\theta(R_w)} , \tag{16}$$

where R_w is the radius of the finite impedance wall. Evidently, the solutions to Eq. (13) are given by

$$\hat{E}_z(r) = \begin{cases} AJ_0(Tr) , & 0 \le r < R_0 , \\ BJ_0(pr) + CN_0(pr) , & R_0 < r \le R_w , \end{cases} \tag{17}$$

where $J_\ell(x)$ and $N_\ell(x)$ are Bessel functions of the first and second kind, respectively, of order ℓ. Making use of Eqs. (7) and (16), and the boundary conditions of $\hat{E}_z(r)$ at $r = R_0$, we obtain the dispersion relation,

$$\frac{\xi J_1(\xi)}{J_0(\xi)} = F(\omega,k) \ , \tag{18}$$

where $F(\omega,k)$ is the wave admittance at the beam surface defined by

$$F(\omega,k) = pR_0 \frac{J_1(pR_0) + g(pR_w)N_1(pR_0)}{J_0(pR_0) + g(pR_w)N_0(pR_0)} \ , \tag{19}$$

and

$$\xi = TR_0 \ . \tag{20}$$

In Eq. (19),

$$g(x) = \frac{J_1(x)}{xN_0(x) - ZN_1(x)} \left(Z - \frac{xJ_0(x)}{J_1(x)} \right) \ , \tag{21}$$

and p is defined in Eq. (14). In the remainder of this article, we make use of Eq. (18) to investigate properties of the space charge wave for various values of wall impedance Z in Eq. (16).

III. INFLUENCE OF WAVE ADMITTANCE ON THE SPACE CHARGE WAVES

For convenience in the subsequent analysis, we denote the root of Eq. (18) by

$$\xi = \xi_r(\omega,k) + i\xi_i(\omega,k) \ , \tag{22}$$

for a specified value of wave admittance

$$F = f\exp(i\phi) = F_r + iF_i \ , \tag{23}$$

where ξ_r and ξ_i are the real and imaginary parts of ξ, and f and ϕ are the magnitude and phase angle, respectively, of the general wave admittance F at the beam surface. From Eq. (18) with Eq. (23), we note

$$\frac{\xi^* J_1(\xi^*)}{J_0(\xi^*)} = f\exp(-i\phi) \ , \tag{24}$$

where ξ^* is the complex conjugate of ξ defined by $\xi^* = \xi_r - i\xi_i$.

Shown in Fig. 1 are contours of constant phase angle ϕ and modulus f of the function $F = \xi J_1(\xi)/J_0(\xi)$ in the complex plane $\xi = \xi_r + i\xi_i$. We note from Fig. 1 that the root ξ of Eq. (18) approaches zero or α_{0n} as the magnitude of the wave admittance is reduced to zero, $f \rightarrow 0$. On the other hand, ξ approaches β_{0n} as f increases to infinity. Here α_{0n} and β_{0n} are the nth root of $J_1(\alpha_{0n}) = 0$ and $J_0(\beta_{0n}) = 0$, respectively. For specified values of f and ϕ, we note that the root $\xi = \xi_r + i\xi_i$ can be determined from Fig. 1.

Within the context of Eq. (1), it is very useful in the subsequent analysis to note that

$$|\omega - k\beta_b c| \ll kc \ . \tag{25}$$

In the remainder of this section, we investigate the resistive wall instability[10] in general, assuming that all electrons have the same value of axial camonical momentum, i.e.,

$$\Delta = 0 \ . \tag{26}$$

Making use of Eqs. (14), (20), and (26), we obtain,

$$\Omega_i^2 = \frac{1}{2[(y+\delta)^2+1]} \left\{ |y|[(y+\delta)^2+1]^{1/2} - y(y+\delta) \right\} , \tag{27}$$

for the resistive wall instability in general. In Eq. (27), Ω_i is the normalized growth rate defined by

$$\Omega_i = \frac{\mathrm{Im}(\omega - k\beta_b c)}{\omega_{pb}/\gamma_b} , \tag{28}$$

and the parameters y and δ are given by

$$y = k^2 R_0^2 / 2\gamma_b^2 \xi_r \xi_i , \tag{29}$$

and

$$\delta = (\xi_r^2 - \xi_i^2)/2\xi_r \xi_i , \tag{30}$$

respectively. In obtaining Eq. (27), use has been made of Eq. (25).

(a) <u>Inductive impedance with $\xi_i^2 > \xi_r^2$</u>. Shown in Fig. 2 are plots of the normalized growth rate Ω_i versus y obtained from Eq. (27) for $\xi_i^2 > \xi_r^2$ and several different values of δ. As shown in Fig. 2, Ω_i^m is the maximum growth rate for a given value of parameter δ, and y_m^I is the corresponding value of y. Obviously from Fig. 2, the maximum growth rate increases rapidly with the increasing value of $|\delta|$ in the inductive impedance case. In Fig. 3, we plot the parameter y_m^I corresponding to the maximum growth rate versus δ (solid line) obtained from Eq. (27) and $y_m^I = -\delta$ (dashed line). Evidently, we note from Fig. 3 that the maximum growth rate Ω_i^m and the corresponding y_m^I can be approximated by

$$\Omega_i^m \simeq (|\delta|/2)^{1/2} , \tag{31}$$

and

$$y_m^I \simeq -\delta , \tag{32}$$

for $|\delta| \geq 1$. Substituting Eqs. (29) and (30) into Eq. (32), we conclude for the inductive impedance that the maximum growth rate of the resistive wall instability occurs at the axial wavenumber k satisfying $k^2R_0^2 = \gamma_b^2(\xi_i^2 - \xi_r^2)$ for $|\delta| \geq 1$.

(b) Capacitive impedance with $\xi_r^2 > \xi_i^2$. Presented in Fig. 4 are plots of the normalized growth rate Ω_i versus y obtained from Eq. (27) for $\xi_r^2 > \xi_i^2$ and several values of parameter δ. As shown in Fig. 4, we again define the maximum growth rate Ω_i^m and corresponding y_m^c for a given value of δ. In order to illustrate the stability dependence on the parameter δ, in Fig. 5, we plot the maximum growth rate Ω_i^m and corresponding y_m^c versus δ obtained from Eq. (27) for $\xi_r^2 > \xi_i^2$. The growth rate increases rapidly with the decreasing value of $|\delta|$ for the capacitive impedance case.

(c) Perfectly resistive with $\xi_r^2 = \xi_i^2$. For the perfactly resistive impedance case characterized by

$$\xi_r^2 = \xi_i^2 , \tag{33}$$

Eq. (27) can be simplified as

$$\Omega_i^2 = \frac{1}{2(y^2+1)} [|y|(y^2+1)^{1/2} - y^2] , \tag{34}$$

which gives the maximum growth rate

$$\Omega_i^m = 0.3536 , \tag{35}$$

at y = 0.577. We therefore conclude that the inductive impedance case is most unstable. In the following sections, we investigate properties of the space charge waves in perfectly capacitive and inductive impedances.

IV. SPACE CHARGE WAVES IN A PERFECTLY CONDUCTING WAVEGUIDE

In this section, we investigate properties of the space charge waves in a relativistic electron beam assuming that the wall impedance is zero, i.e.,

$$Z = 0 \ , \tag{36}$$

and that all electrons have the same value of axial canonical momentum ($\Delta = 0$). Substituting Eqs. (21) and (36) into Eq. (19) and defining

$$q^2 = (k^2 - \omega^2/c^2)R_0^2 \ , \tag{37}$$

we obtain

$$F(q) = q\,\frac{I_1(q)K_0(R_w q/R_0) + I_0(R_w q/R_0)K_1(q)}{I_0(R_w q/R_0)K_0(q) - I_0(q)K_0(R_w q/R_0)} \ , \tag{38}$$

where $I_\ell(x)$ and $K_\ell(x)$ are the modified Bessel functions of the first and second kind, respectively, of order ℓ. For a real value of q, the wave admittance F(q) in Eq. (38) is a positive real value ($F_i = 0$), thereby giving the phase angle $\phi = 0$ in Eq. (23). In this regard, the space charge wave admittance F in a perfectly conducting waveguide is a perfactly capacitive, corresponding to the horizontal line $\xi_i = 0$ in Fig. 1. Without further analysis, we therefore conclude from Fig. 4 that the space charge mode in a perfectly conducting waveguide is stable [$\delta = \infty$ in Eq. (27)].

Figure 6 shows plots of the admittance $F = F_r$ versus $\xi = \xi_r$ (dashed curves) obtained from Eq. (18) and F_r versus q (solid curves) obtained from Eq. (38) for $R_0/R_w = 0.1$, 0.5 and 0.9. The horizontal scale in Fig. 6 represents both ξ_r and q. In Fig. 6, n = 1, 2, and 3 denote the radial mode number of the space charge wave. Note that for specified values of q and R_w/R_0, the parameter ξ_r is determined from Fig. 6. Shown in Fig. 7 is plot of ξ_r versus q determined from Fig. 6 for $R_0/R_w = 0.5$. Obviously, the root ξ_r approaches β_{0n} as the parameter q increases to infinity. This is similar to Fig. 1, since the wave admittance F_r is monotonically increasing with the increasing value of q.

In order to illustrate the influence of the parameter q on the space charge mode, we present in Fig. 8 plots of the eigenfunction $\hat{E}_z(r)$ versus r/R_0 obtained from Eq. (17) for (a) n = 1, (b) n = 2, $R_0/R_w = 0.5$ and several values of q. The perturbed axial electric field $\hat{E}_z(r)$ in Fig. 8 is normalized by

$$\frac{1}{R_0^2}\int_0^{R_w} dr\, r\, \hat{E}_z(r) = 1.$$

It is obvious from Fig. 8 that the axial electric field $\hat{E}_z(r)$ in Eq. (17) can be approximated by

$$\hat{E}_z(r) \simeq \begin{cases} AJ_0(\beta_{0n} r/R_0) , & 0 \le r < R_0 , \\ 0 , & \text{otherwise} , \end{cases} \tag{39}$$

for $q \gtrsim 10$. We therefore conclude that inside the beam, the electrostatic eigenfunction of the large axial wavenumber perturbations is represented by a Bessel function. For example, Eq. (39) is an excellent approximation for the electrostatic eigenfunction of the free electron laser instability.[7,8]

Making use of Eq. (20) and (37), Eq. (14) can be expressed as

$$(\omega - k\beta_b c)^2 = \frac{\omega_{pb}^2 q^2}{\gamma_b^2(\xi_r^2 + q^2)} , \tag{40}$$

where the root $\xi_r(q)$ is determined from Fig. 7 for given values of R_0/R_w and n, and use has been made of $\Delta = 0$. The eigenfrequency ω and axial wavenumber k are obtained from the simultaneous solution of

Eqs. (37) and (40). Shown in Fig. 9 is a plot of the dispersion curve in the (ω,k) parameter space for $n = 1$, $R_0/R_w = 0.5$, $\gamma_b = 3$, and $\nu/\gamma_b = \omega_{pb}^2 R_0^2/4c^2 = 0.1$. Simultaneously solving Eqs. (37) and (40) for q and $\xi_r(q)$ give two distinct dispersion curves. The fast wave mode in Fig. 9 corresponds to the phase velocity $V_{ph} = \omega/k > \beta_b c$ and the slow wave mode corresponds to $V_{ph} < \beta_b c$.

After some straightforward algebraic manipulation with the definition $\nu/\gamma_b = \omega_{pb}^2 R_0^2/4c^2$ we can rewrite Eq. (40) by

$$\left(\frac{\omega}{kc} - \beta_b\right)^2 = \frac{4\nu}{\gamma_b^3} \frac{1 - \omega^2/k^2c^2}{\xi_r^2 + (1 - \omega^2/k^2c^2)k^2R_0^2} , \tag{41}$$

which determines the phase velocity $V_{ph} = \omega/k$ of the space charge wave in terms of the normalized axial wavenumber kR_0, the Budker's parameter ν and energy γ_b of the electron beam. In recent years, there has been a considerable increase in interest in collective ion acceleration by a slow space-charge wave[3-6] in a relativistic electron beam. However, the phase velocity of the space charge wave is initially required to be zero, in order to trap and accelerate ions. In this regard, we derive the condition for $V_{ph} = \omega/k = 0$ from Eq. (41). That is,

$$\frac{4\nu}{\gamma_b} = (\gamma_b^2 - 1)[\xi_r^2(kR_0) + k^2R_0^2] , \tag{42}$$

where the root ξ_r is determined in terms of the normalized axial wavenumber kR_0. For given values of R_0/R_w and n, the root ξ_r required in Eq. (42) can be found from Fig. 7 where the horizontal scale q is replaced by kR_0.

Figure 10 is plots of ξ_r versus R_0/R_w for $n = 1$ and several values of kR_0. The root ξ_r is monotonically increasing to $\epsilon_{01} = 2.4$ as the ratio R_0/R_w increases from zero to unity. Making use of Fig. 10, the necessary value of Budker's parameter for the zero phase velocity of space charge wave is found from Eq. (42). For example, for $kR_0 = 1$, $R_0/R_w = 0.5$ and $\gamma_b = 1.2$, we find $4\nu/\gamma_b = 1.46$ for $V_{ph} = \omega/k = 0$. Typical Budker's parameter for the zero phase velocity is order of unity in a practical range of physical parameters for collective ion acceleration. Finally, for a small phase velocity satisfying $|\omega/kc| << \beta_b$, Eq. (41) can be approximated by

$$\frac{4\nu}{\gamma_b} \simeq (\gamma_b^2 - 1)\left[\xi_r^2 + \left(\frac{\omega R_0}{c}\right)^2\left(\frac{kc}{\omega}\right)^2\right] , \qquad (43)$$

which is identical to Eq. (42). However, from Eq. (43), the Budker's parameter is determined in terms of the oscillation frequency ω and the phase velocity $V_{ph} = \omega/k$ required to ion accelerations.

V. SPACE CHARGE WAVES FOR A DIELECTRIC LOADED WAVEGUIDE

In this section, we investigate properties of the space charge waves for a solid electron beam in a dielectric loaded waveguide. The solid electron beam with radius R_0 propagates through a cylindrical waveguide loaded with dielectric material in the range $R_w < r < R_c$. A grounded cylindrical conducting wall is located at radius R_c. We approximate the permeability of a dielectric material $\mu = 1$. In this regard, the perturbed axial electric field $\hat{E}_z(r)$ and azimuthal magnetic field $\hat{B}_\theta(r)$ are continuous across the dielectric boundary at $r = R_w$. From Eq. (8), we obtain

$$\left(\frac{1}{r}\frac{\partial}{\partial r} r \frac{\partial}{\partial r} + p_2^2\right)\hat{E}_z(r) = 0 , \tag{44}$$

inside the dielectric material ($R_w \le r \le R_c$). Here p_2 is defined by

$$p_2^2 = \omega^2\varepsilon/c^2 - k^2 . \tag{45}$$

The solution to Eq. (44) can be expressed as

$$\hat{E}_z(r) = A[J_0(p_2 r) - J_0(p_2 R_c)N_1(p_2 r)/N_0(p_2 R_c)] , \tag{46}$$

where A is an arbitrary constant. Substituting Eq. (46) into Eq. (7), and making use of the boundary conditions at $r = R_w$ and Eq. (16), we obtain the impedance

$$Z = \frac{\eta}{\varepsilon}\,\frac{J_0(\eta)N_0(\eta R_c/R_w) - J_0(\eta R_c/R_w)N_0(\eta)}{J_1(\eta)N_0(\eta R_c/R_w) - J_0(\eta R_c/R_w)N_1(\eta)} , \tag{47}$$

at the surface of dielectric material ($r = R_w$). In Eq. (47), the parameter η is defined by

$$\eta^2 = p_2^2 R_w^2 = R_w^2(\omega^2\varepsilon/c^2 - k^2) . \tag{48}$$

Equation (18), when combined with Eqs. (19), (21), and (47), yields a closed dispersion relation for the space charge wave mode in a dielectric loaded waveguide.

Making use of Eqs. (14), (19), and (20), it can be shown that in the vacuum dielectric waveguide characterized by $\omega_{pb}^2 = 0$ in Eq. (14), the dispersion relation in Eq. (18) is simplified as

$$g(pR_w) = 0 \,, \tag{49}$$

where $p = (\omega^2/c^2 - k^2)^{1/2}$. Substituting Eqs. (21) and (47) into Eq. (49), we obtain the vacuum transverse magnetic (TM) mode dispersion relation,

$$\frac{pR_w J_0(pR_w)}{J_1(pR_w)} = \frac{\eta}{\varepsilon} \frac{J_0(\eta)N_0(\eta R_c/R_w) - J_0(\eta R_c/R_w)N_0(\eta)}{J_1(\eta)N_0(\eta R_c/R_w) - J_0(\eta R_c/R_w)N_1(\eta)} \,, \tag{50}$$

where the parameter pR_w is defined by

$$p^2R_w^2 = R_w^2(\omega^2/c^2 - k^2) \,. \tag{51}$$

It is instructive to examine Eq. (50) in the limit $\varepsilon \to 1$. Making use of $pR_w = \eta$, we obtain

$$J_0(\eta R_c/R_w) = 0 \,, \tag{52}$$

from Eq. (50) for $\varepsilon = 1$. Equation (52) gives the familiar vacuum TM mode dispersion relation,

$$\frac{\omega^2}{c^2} - k^2 = \frac{\beta_{0n}^2}{R_c^2} \,, \tag{53}$$

in a perfectly conducting waveguide. Moreover, we can show that in the limit of both $R_w \to R_c$ and $R_w \to 0$, Eq. (50) gives the dispersion relation in Eq. (53) and,

$$\frac{\omega^2}{c^2}\varepsilon - k^2 = \frac{\beta_{0n}^2}{R_c^2} \,, \tag{54}$$

respectively. Note that the case $R_w \rightarrow 0$ corresponds to a completely filled dielectric waveguide.

For given values of the dielectric constant ε and the ratio R_w/R_c, the parameter pR_w is determined from Eq. (50) in terms of η. The oscillation frequency ω and axial wavenumber k in a vacuum dielectric loaded waveguide are obtained from the simultaneous solution of Eqs. (48) and (51) for specified η and pR_w. Figure 11 is plots of the vacuum TM mode dispersion relation in the (ω,k) parameter space for (a) $R_w/R_c = 0.8$ and several values of the dielectric constant ε, and (b) $\varepsilon = 4$ and several values of the ratio R_w/R_c. We remind the reader that the thickness of dielectric material increases from zero to R_c as the ratio R_w/R_c decreases from unity to zero. All plots in Fig. 11 correspond to the first radial mode number (n = 1). The dispersion curve for $R_w/R_c = 0$ in Fig. 11(b) represents the dispersion relation of a completely filled dielectric waveguide [Eq. (54)]. On the other hand, the curves for $\varepsilon = 1$ in Fig. 11(a) and for $R_w/R_c = 1$ in Fig. 11(b) correspond to the ordinary dispersion relation in Eq. (53) where the phase velocity $V_{ph} = \omega/k$ is always faster than the speed of light $(\omega/k > c)$. However, the phase velocity of the dispersion relation in a dielectric loaded waveguide is sometimes less than the speed of light $(\omega/k < c)$. For example, for $R_w/R_c = 0.8$ and $\varepsilon = 4$ in Fig. 11(a), we find $\omega/k > c$ for $kR_c < 3.3$ and $\omega/k < c$ for $kR_c > 3.3$.

It is evident from Eq. (14) and (20) that in the vacuum dielectric waveguide $(\omega_{pb}^2 = 0)$, we can equivalently express the combination of Eqs. (48), (50), and (51) as,

$$\frac{\omega^2}{c^2} - k^2 = \xi^2(\omega,k)/R_0^2 , \tag{55}$$

where $\xi(\omega,k)$ is determined from Eq. (18) in terms of the wave admittance F at $r = R_0$. Equation (55) is a compact form of the vacuum TM mode dispersion relation in a dielectric loaded waveguide. Shown in Fig. 12 is a plot of $\omega = (k^2c^2 + \beta_{0n}^2c^2/R_c^2)^{1/2}$ versus k corresponding to a perfectly conducting waveguide and $\omega = (k^2c^2 + \xi^2c^2/R_0^2)^{1/2}$ versus k corresponding to a dielectric loaded waveguide. The straight line $\omega = k\beta_b c$ represents the free-streaming mode. In a range of physical parameters, the mode $\omega = k\beta_b c$ intersects $\omega = (k^2c^2 + \xi^2c^2/R_0^2)^{1/2}$ at $k = k_p$, indicating a possible mode coupling. In fact, for $k > k_p$ in Fig. 12, the phase velocity of the vacuum dielectric mode is less than the beam velocity. In this regard, we expect a strong Cherenkov radiation[10,11] near the intersection point of these two modes.

In order to investigate stability properties of the space charge wave in a dielectric loaded waveguide, it is necessary to numerically solve Eq. (18) with no a priori assumption that the beam is very tenuous. However, use is made of the fact that the Doppler-shifted eigenfrequency $\omega - k\beta_b c$ is well removed from the free-streaming mode, i.e., $|\omega - k\beta_b c| \ll k\beta_b c$. Evaluating the parameter η in Eq. (47) and the wave admittance F in Eq. (19) at $\omega = \omega_0 = k\beta_b c$, the dispersion relation in Eq. (18) can be approximated by

$$\frac{(\xi_0 + \delta\xi)J_1(\xi_0 + \delta\xi)}{J_0(\xi_0 + \delta\xi)} = F_0 + (\partial F/\partial\omega)_{\omega_0} (\omega - k\beta_b c) \ , \qquad (56)$$

where

$$F_0 = F(\omega_0,k) \ , \qquad (57)$$

the parameter $\xi_0 = \xi(\omega_0)$ is defined by

$$\frac{\xi_0 J_1(\xi_0)}{J_0(\xi_0)} = F_0 \ , \qquad (58)$$

and

$$\delta\xi = \xi - \xi_0 \ . \qquad (59)$$

Taylor expanding the left-hand side of Eq. (56) about $\xi = \xi_0$ and making use of Eq. (58), we approximate Eq. (56) by

$$\xi^2 = \xi_0^2 \left[1 + \frac{2}{\xi_0^2 + F_0^2} (\partial F/\partial\omega)_{\omega_0} (\omega - k\beta_b c)\right] , \qquad (60)$$

where use has been made of the assumption that the term proportional to $(\partial F/\partial\omega)_{\omega_0}$ in Eq. (60) is much less than unity. Substituting Eqs. (14) and (20) into Eq. (60), we finally have the dispersion relation,

$$\left\{\frac{\omega_{pb}^2}{\gamma_b^2(\omega - k\beta_b c + ik\Delta/\gamma_b^3 m)^2} - 1\right\} \left(k^2 - \frac{\omega^2}{c^2}\right) R_0^2$$
$$= \xi_0^2 \left[1 + \frac{2}{\xi_0^2 + F_0^2} (\partial F/\partial\omega)_{\omega_0} (\omega - k\beta_b c)\right] , \qquad (61)$$

for the space charge wave in a dielectric loaded waveguide.

Defining the normalized Doppler-shifted eigenfrequency Ω by

$$\Omega = \frac{\omega - k\beta_b c}{\omega_{pb}/\gamma_b} , \qquad (62)$$

the dispersion relation in Eq. (61) is numerically investigated for a broad range of physical parameters. For present purposes, to illustrate the mode coupling of the space charge wave ($\omega = k\beta_b c$) with the vacuum dielectric mode, shown in Fig. 13 are plots of (a) F_0 (solid curve) and ξ_0^2 (dashed curve), (b) the normalized growth rate $\Omega_i = \mathrm{Im}\Omega$ and (c) Doppler-shifted real oscillation frequency $\Omega_r = \mathrm{Re}\Omega$ versus kR_0 obtained from Eqs. (57), (58), and (61), for $\gamma_b = 2$, $\epsilon = 8$, $R_0/R_w = 0.8$, $R_w/R_c = 0.8$, and $\nu = 0.0025$. The real oscillation frequency in Fig. 13(c) is obtained for zero axial momentum spread ($\Delta = 0$). In Fig. 13(c), the solid curve represents the unstable mode and the dashed curves correspond to stable oscillations. Several points are noteworthy in

Fig. 13. First, the maximum growth rate for instability occurs at $kR_0 \simeq \gamma_b(-\xi_0^2)^{1/2}$ corresponding to the mode coupling point k_p in Fig. 12. This is consistent with the inductive impedance in Sec. III. For example, in Fig. 13, the maximum coupling occurs at $kR_0 \simeq 2$ and $\xi_0^2 = -1$. Second, the maximum growth rate is order of the beam plasma frequency, indicating a strong instability. In this regard, this instability can be utilized to generate high power microwave. Third, wavelength of the microwave radiation generated by this instability can be less than a centimeter for a subcentimeter beam radius. Fourth, from Fig. 13(c), we note that the Doppler-shifted real frequency Ω_r for instability is negative, thereby implying that the phase velocity of unstable mode is less than the beam velocity. We therefore conclude that the instability mechanism is a typical Cherenkov radiation.[11] Finally, the growth rate and bandwidth of instability decrease with increasing value of the axial momentum spread.

The dependence of stability properties on the ratio R_0/R_w is further illustrated in Fig. 14, where the normalized growth rate $\Omega_i = \mathrm{Im}\Omega$ is plotted versus kR_0 for $\Delta = 0$, several values of R_0/R_w, and parameters otherwise identical to Fig. 13. Obviously from Fig. 14, we note that the growth rate and bandwidth of instability increase rapidly as the surface of dielectric material approaches to the beam surface ($R_0/R_w \to 1$) for a given beam radius. Shown in Fig. 15 is plots of the normalized growth rate versus kR_0 obtained from Eq. (61) for $\gamma_b = 1.1547$, $\varepsilon = 25$, and parameters otherwise identical to Fig. 13(b). Even for a moderate beam energy, the growth rate of instability is also order of the beam plasma frequency. However, the maximum growth rate of instability is rapidly decreasing with increasing value of the axial momentum spread.

Finally, we conclude this section by pointing out that from Figs. 13(a) and (b), the maximum coupling of instability occurs when the wave admittance F_0 is negative [the phase angle $\phi = \pi$ in Eq. (23)]. In this regard, the root ξ can be a pure imaginary value (the $\xi_r = 0$ vertical line in Fig. 1). We therefore emphasize that the wave admittance F in a dielectric loaded waveguide can be perfectly inductive in a range of the axial wavenumber k corresponding to instability.

VI. CONCLUSIONS

In this paper we have investigated properties of the space charge wave in a solid relativistic electron beam propagating in a cylindrical waveguide with an arbitrary impedance Z. The perturbation analysis was carried out within the framework of the linearized Vlasov-Maxwell equations, assuming that $\nu/\gamma_b << 1$. The formal dispersion relation of the space charge wave for azimuthally symmetric electromagnetic perturbations ($\partial/\partial\theta = 0$) was carried out in Sec. II, including the important influence of finite wall impedance Z. In Sec. III, the resistive wall instability with an arbitrary impedance was investigated, showing that an inductive impedance wall is most unstable. Particularly, the maximum growth rate of the general resistive wall instability occurs at the axial wavenumber k satisfying $2k^2R_0^2 = \gamma_b^2(\xi_i^2 - \xi_r^2)$. Properties of the space charge wave in a perfectly conducting waveguide was investigated in Sec. IV. It was found that the space charge wave admittance in a perfactly conducting waveguide is purely capacitive, thereby indicating a stable propagation of the electromagnetic wave. Moreover, we obtained the condition for the zero phase velocity ($\omega/k = 0$), in connection with collective ion acceleration. Furthermore, it was also shown in Sec. IV that for short axial wavelength perturbations ($kR_0/\gamma_b \gtrsim 10$), the eigenfunction can be represented by a Bessel function. Space charge wave properties for a dielectric loaded waveguide were investigated in Sec. V. It was found that a strong mode coupling between the vacuum dielectric waveguide and beam streaming modes occurs in a range of physical parameters, exhibiting possibilities of a strong Cherenkov radiation. The maximum growth rate of instability is order of the beam plasma frequency. In this regard, the Cherenkov radiation can also be an effective means to produce intense high power microwave. The wavelength of the microwave radiation can be less than a centimeter.

ACKNOWLEDGMENTS

This research was supported by the Independent Research Fund at the Naval Surface Weapons Center.

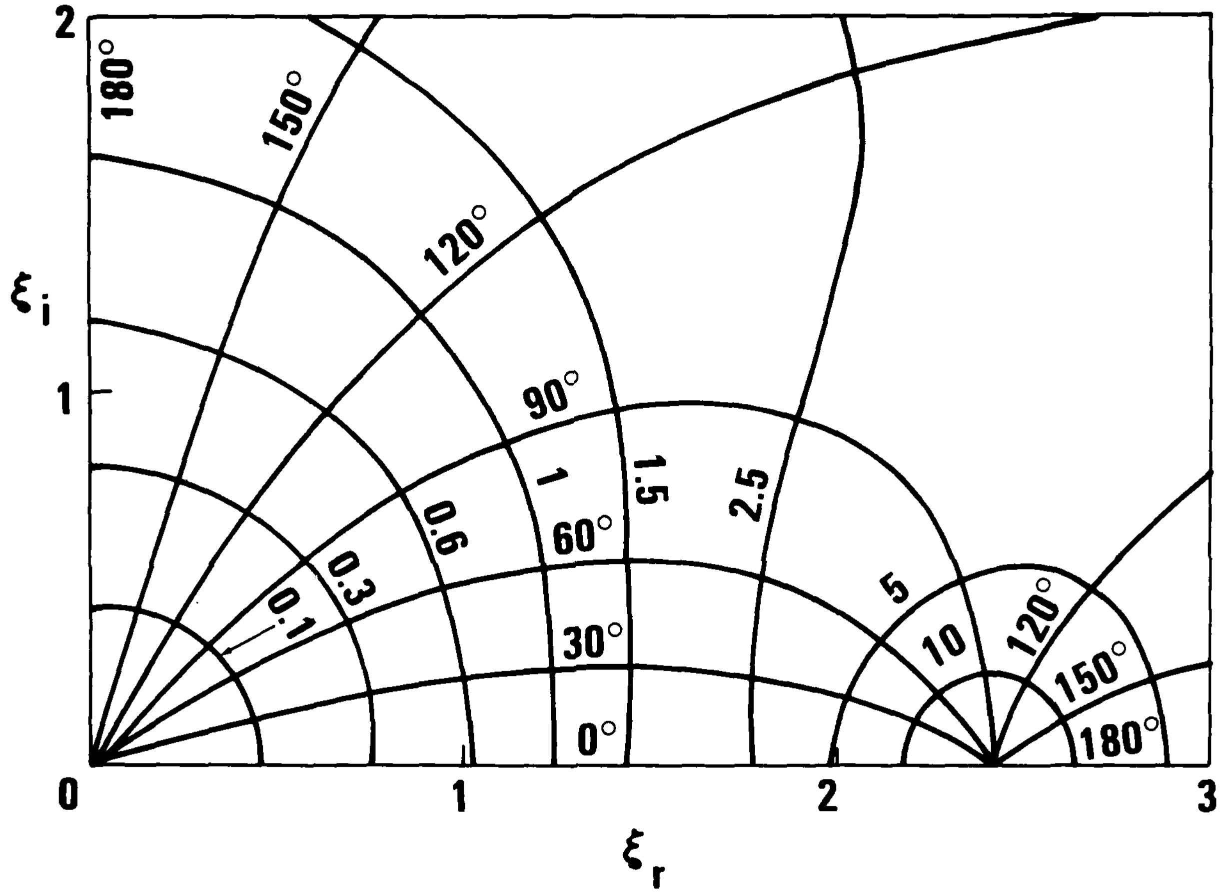

FIGURE 1 CONTOURS OF CONSTANT PHASE ANGLE ϕ AND MODULUS f [EQ. (18)] IN THE COMPLEX PLANE $\xi = (\xi_r, \xi_i)$ FOR n = 1 RADIAL MODE NUMBER.

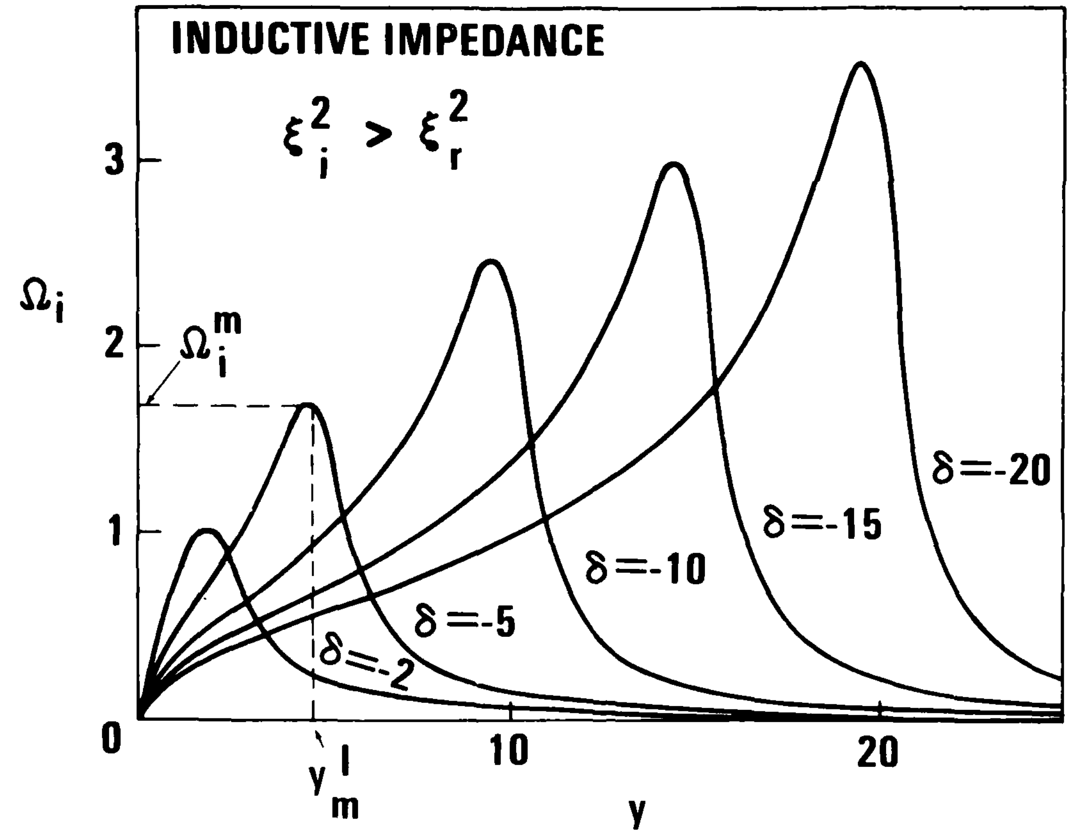

FIGURE 2 PLOT OF THE NORMALIZED GROWTH RATE Ω_i VERSUS y [EQ. (27)] FOR $\xi_i^2 > \xi_r^2$ AND SEVERAL VALUES OF δ.

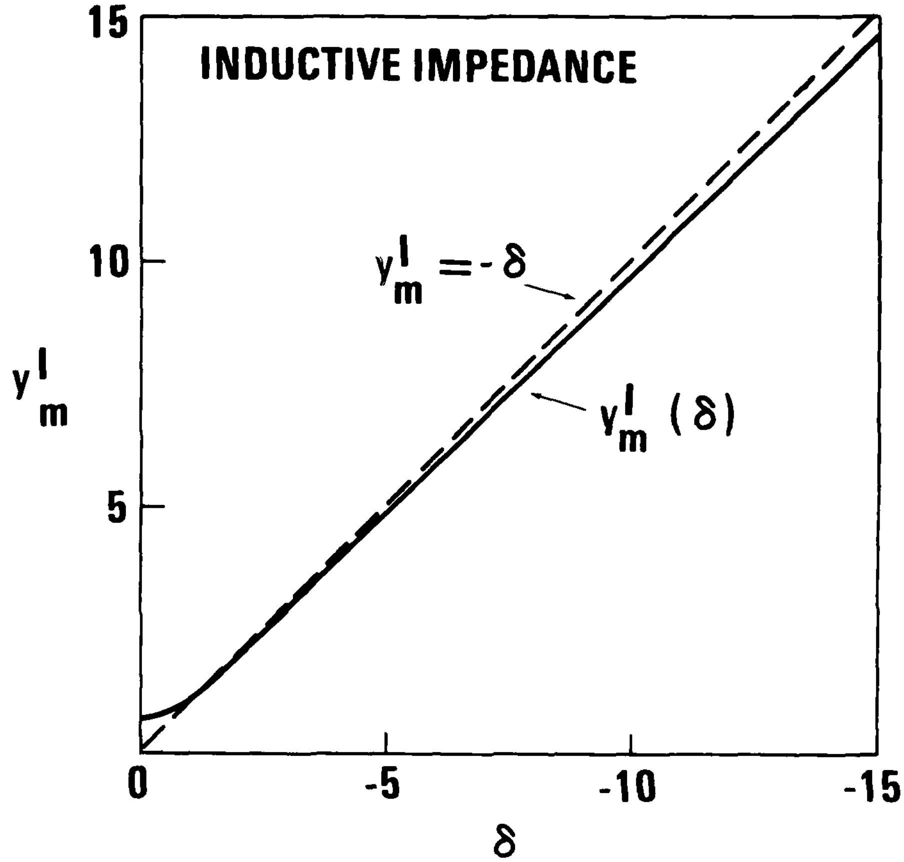

FIGURE 3 PLOT OF THE PARAMETER y_m^I VERSUS δ (SOLID CURVE) OBTAINED FROM EQ. (27) FOR $\xi_i^2 > \xi_r^2$. THE DASHED STRAIGHT LINE IS $y_M^I = -\delta$.

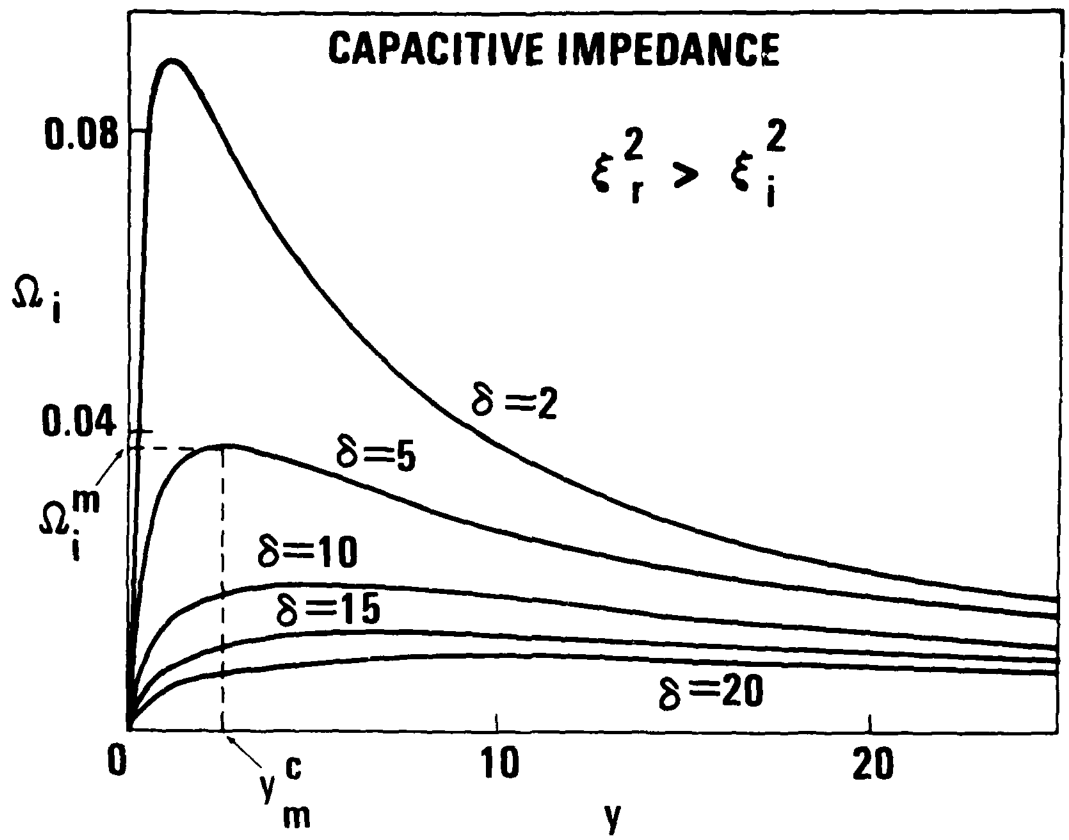

FIGURE 4 PLOT OF THE NORMALIZED GROWTH RATE Ω_i VERSUS y [EQ. (27)] FOR $\xi_r^2 > \xi_i^2$ AND SEVERAL VALUES OF δ.

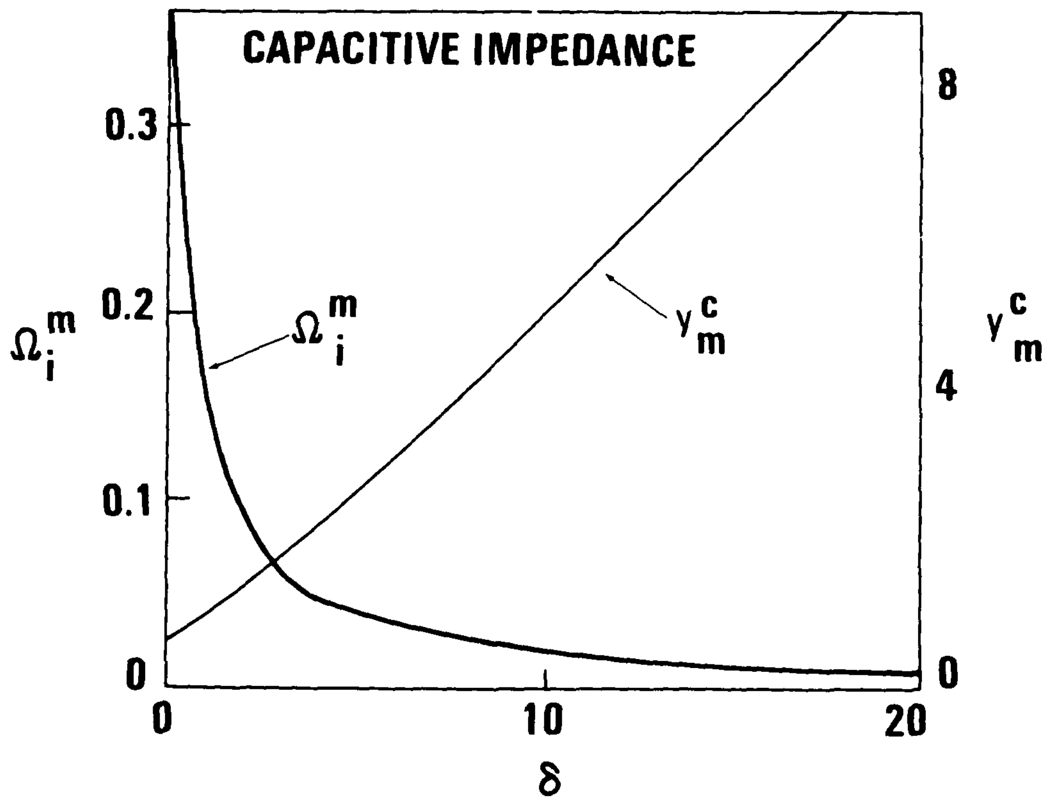

FIGURE 5 PLOT OF THE NORMALIZED MAXIMUM GROWTH RATE Ω_i AND CORRESPONDING y_m^c VERSUS δ [EQ. (27)] FOR $\xi_r^2 > \xi_i^2$.

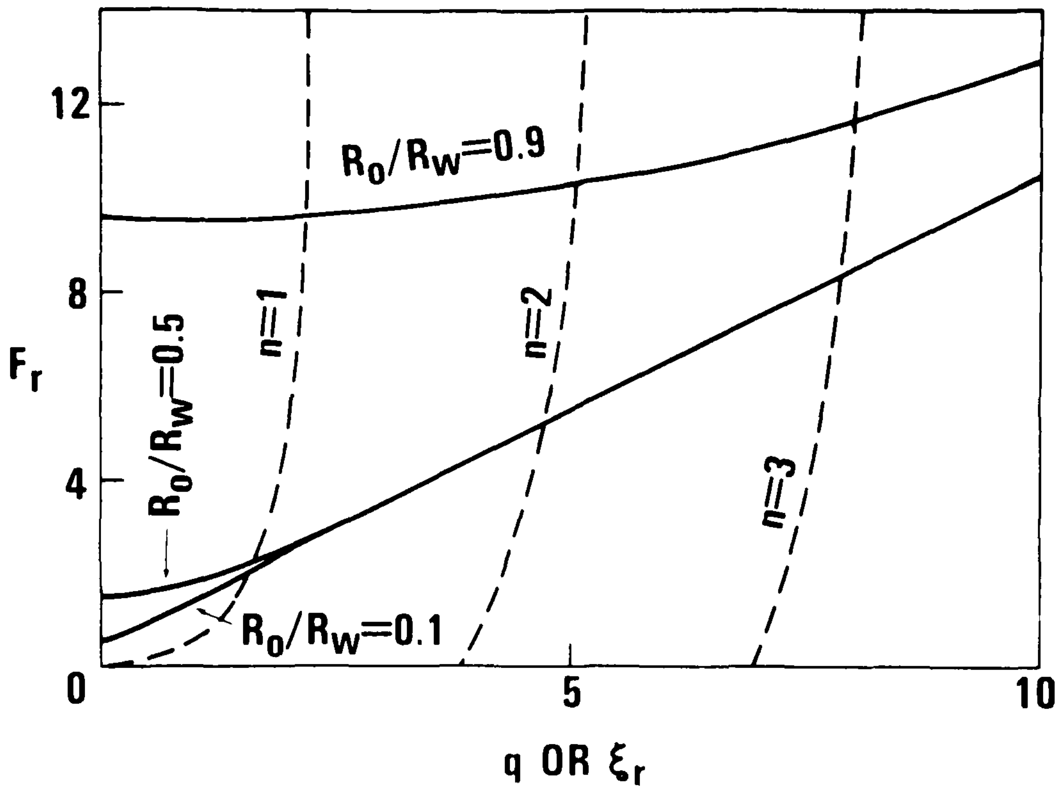

FIGURE 6 PLOT OF THE ADMITTANCE $F = F_r$ VERSUS $\xi = \xi_r$ (DASHED CURVES) OBTAINED FROM EQ. (18) AND F_r VERSUS q (SOLID CURVES) OBTAINED FROM EQ. (38) FOR R_0/R_w = 0.1, 0.5, AND 0.9. THE HORIZONTAL SCALE REPRESENTS BOTH ξ_r AND q.

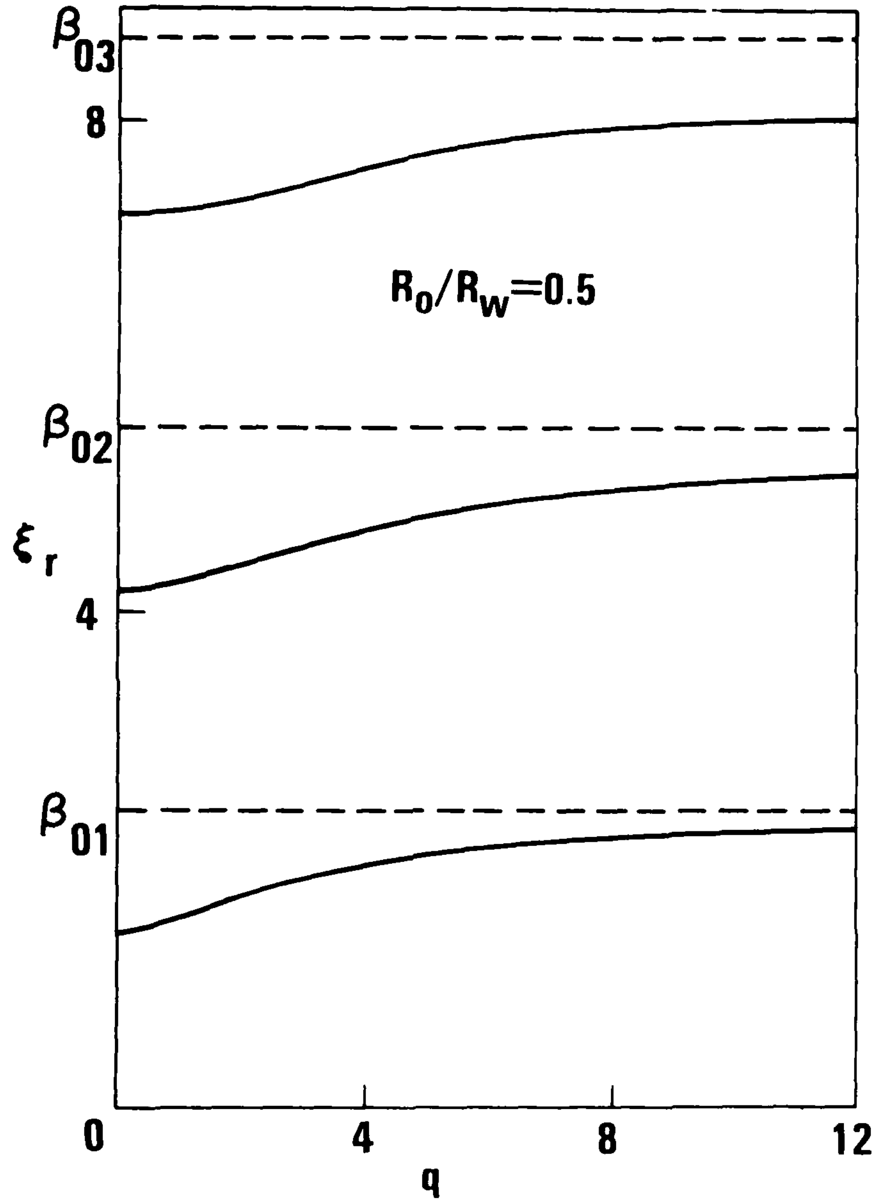

FIGURE 7 PLOT OF ξ_r VERSUS q DETERMINED FROM FIGURE 6 FOR R_0/R_w = 0.5.

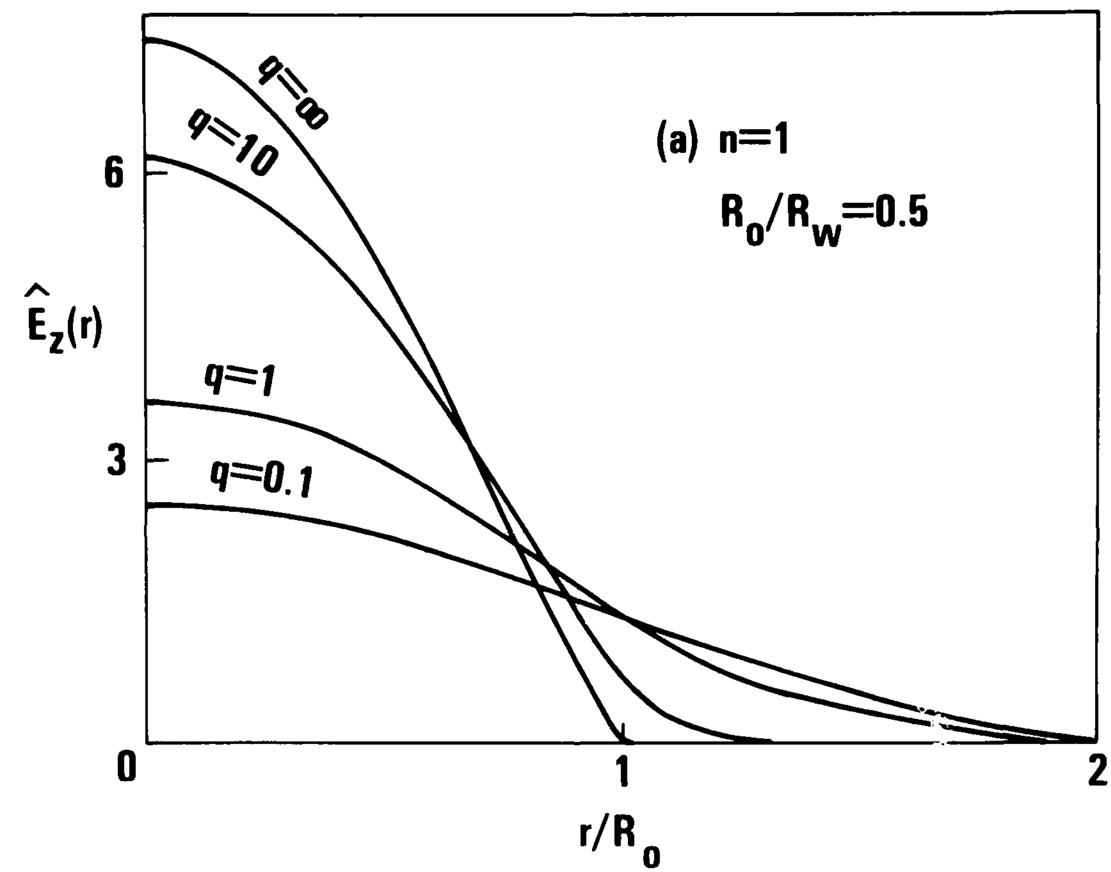

FIGURE 8a PLOT OF THE EIGENFUNCTION $\hat{E}_z$ (r) VERSUS r/R_0 [EQ. (17)] FOR $n = 1$, $R_0/R_W = 0.5$, AND SEVERAL VALUES OF q.

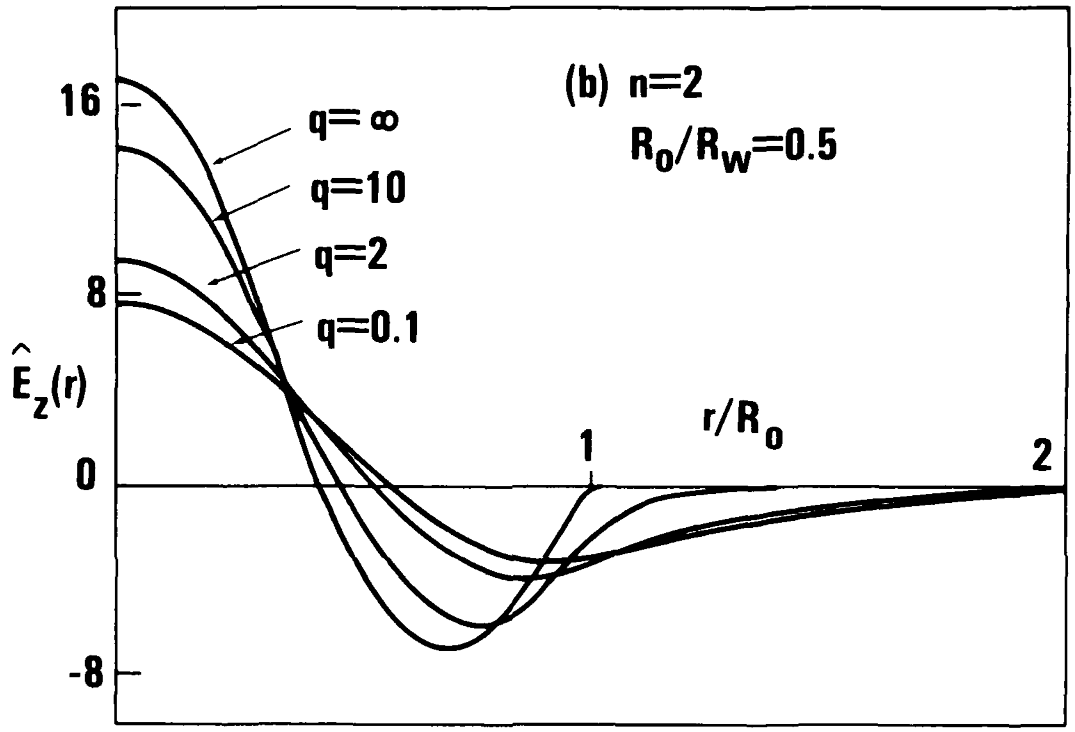

FIGURE 8b PLOT OF THE EIGENFUNCTION $\hat{E}_z$ (r) VERSUS r/R_0 [EQ. (17)] FOR n = 2, R_0/R_w = 0.5, AND SEVERAL VALUES OF q.

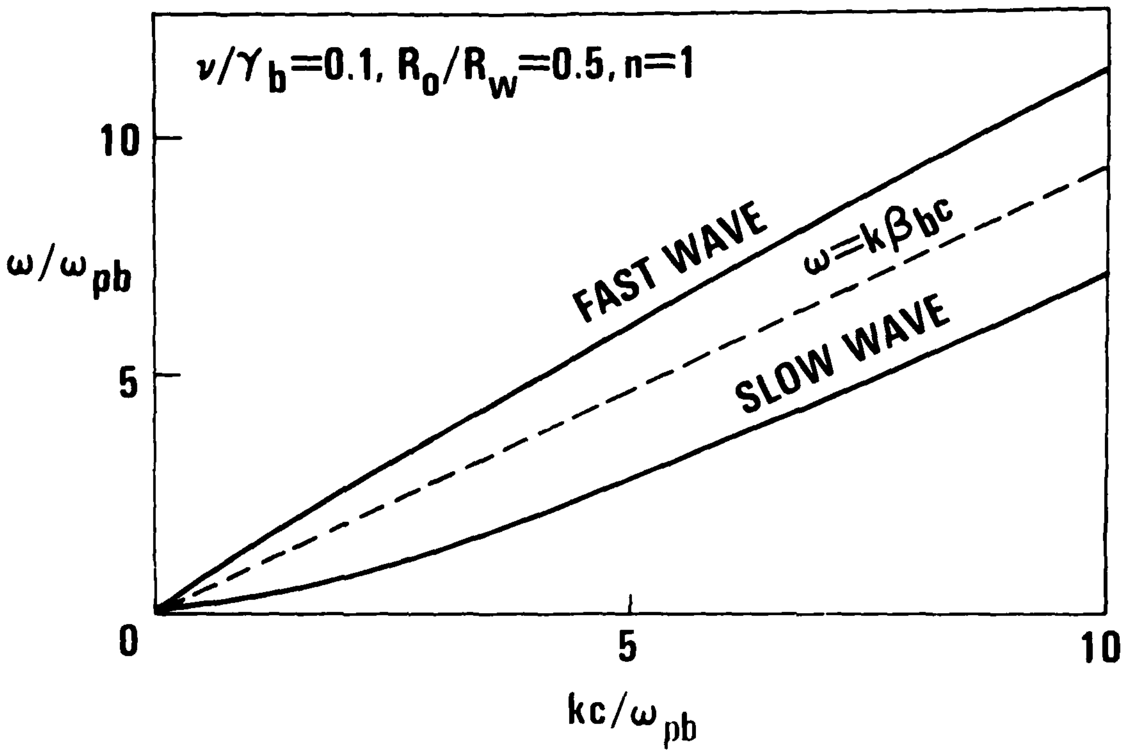

FIGURE 9 PLOT OF THE DISPERSION CURVE IN THE PARAMETER SPACE (ω, k) FOR $n = 1$, $R_0/R_w = 0.5$, $\gamma_b = 3$, AND $\upsilon/\gamma_b = 0.1$. THE DASHED STRAIGHT LINE $\omega = k\beta_b c$ IS THE FREE-STREAMING MODE.

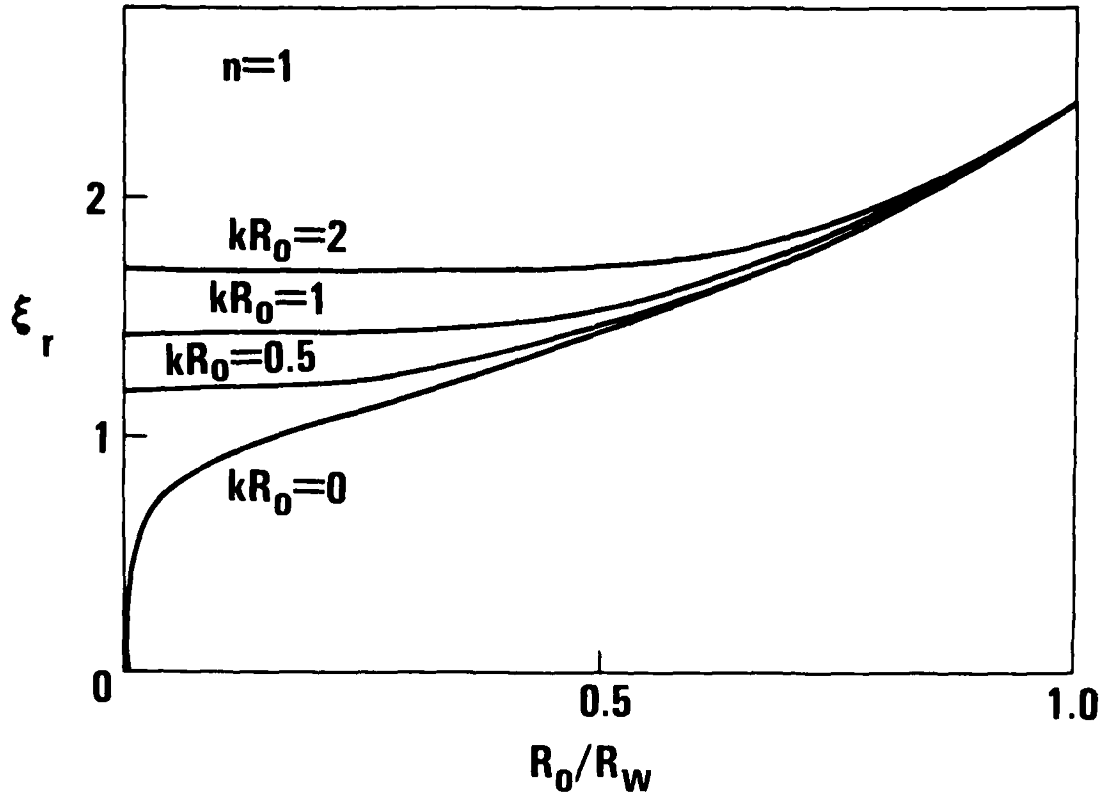

FIGURE 10 PLOT OF ξ_r [REQUIRED IN EQ. (42)] VERSUS R_0/R_w FOR n = 1 AND SEVERAL VALUES OF kR_0.

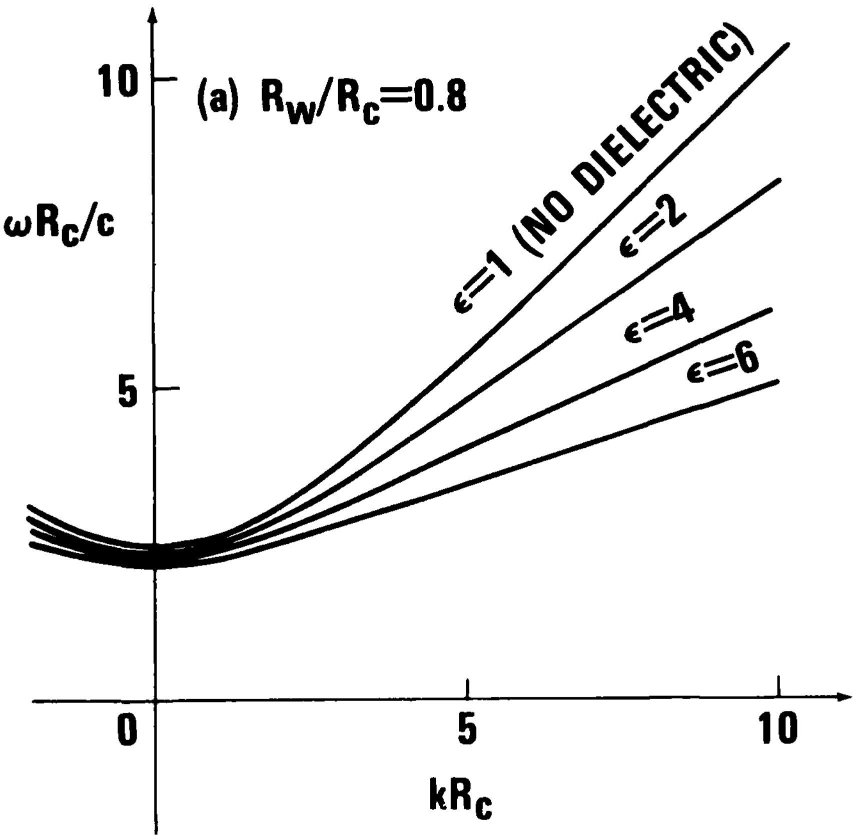

FIGURE 11a PLOT OF THE VACUUM TM MODE DISPERSION RELATION IN THE PARAMETER SPACE (ω,k) OBTAINED FROM EQS. (48), (50), AND (51) FOR R_W/R_c = 0.8 AND SEVERAL VALUES OF THE DIELECTRIC CONSTANT ϵ.

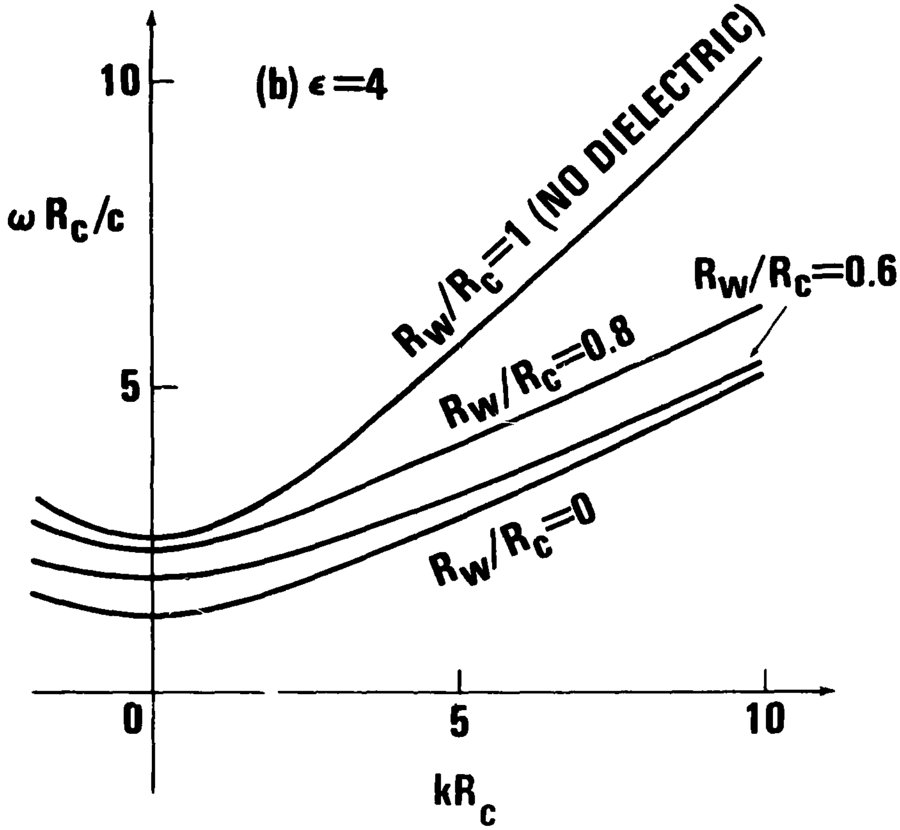

FIGURE 11b PLOT OF THE VACUUM TM MODE DISPERSION RELATION IN THE PARAMETER SPACE (ω,k) OBTAINED FROM EQS. (48), (50), AND (51) FOR $\epsilon = 4$ AND SEVERAL VALUES OF THE RATIO R_w/R_c.

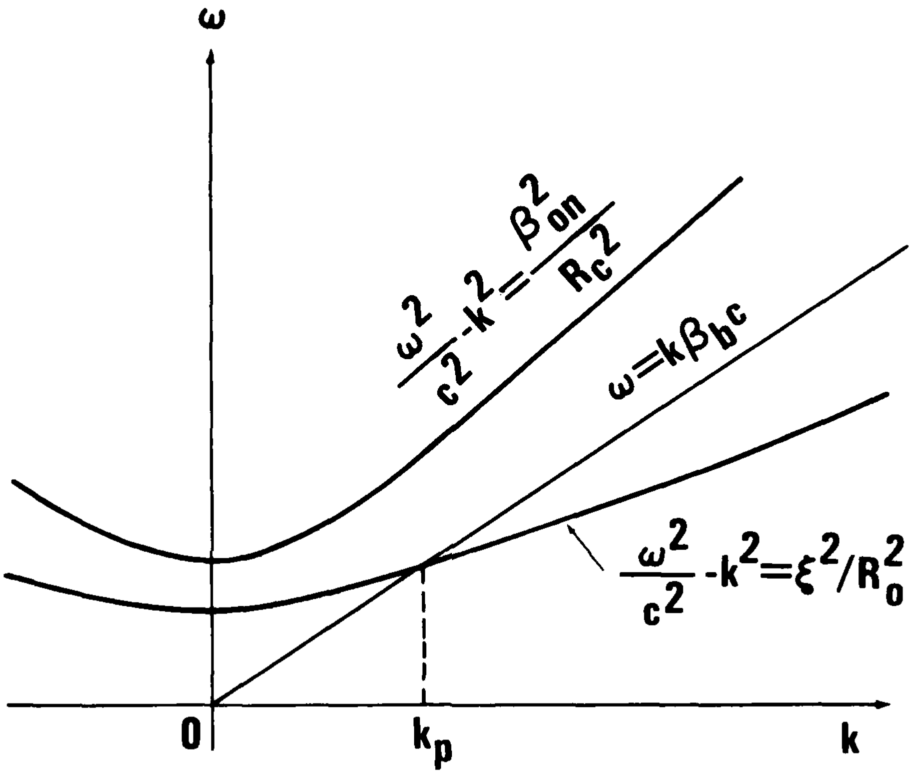

FIGURE 12 SKETCH OF $\omega = (k^2c^2 + \beta_{0n}^2 c^2/R_c^2)^{1/2}$ VERSUS k (CORRESPONDING TO PERFECTLY CONDUCTING WAVEGUIDE) AND $\omega = (k^2c^2 + \xi^2 c^2/R_0^2)^{1/2}$ VERSUS k (CORRESPONDING TO AN ARBITRARY WALL IMPEDANCE Z). THE STRAIGHT LINE $\omega = k\,\beta_b c$ IS THE FREE-STREAMING MODE.

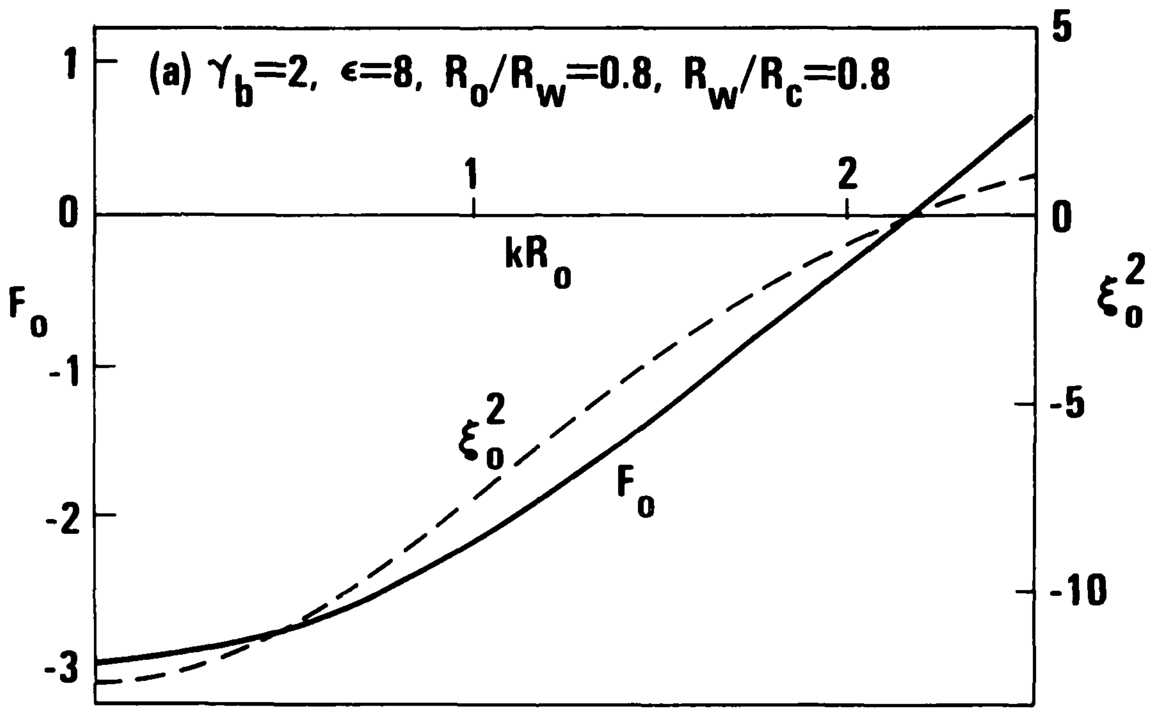

FIGURE 13a PLOTS OF F_0 (SOLID CURVE) AND ξ_0^2 (DASHED CURVE), [EQS. (57), (58), AND (61)] FOR $\gamma_b = 2$, $\epsilon = 8$, $R_0/R_w = 0.8$, $R_w/R_c = 0.8$, AND $\upsilon = 0.0025$. THE REAL OSCILLATION FREQUENCY IS OBTAINED FOR $\Delta = 0$.

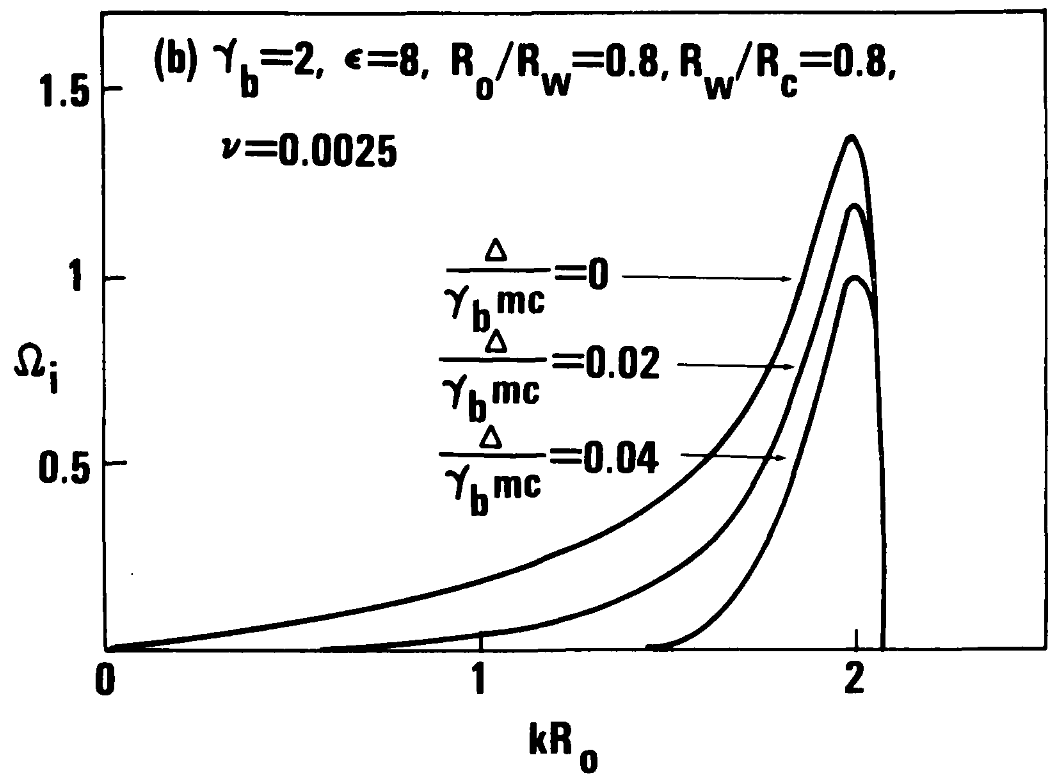

FIGURE 13b PLOTS OF THE NORMALIZED GROWTH RATE Ω_i = 1mΩ [EQS. (57), (58), AND (61)] FOR γ_b = 2, ϵ = 8, R_0/R_w = 0.8, R_w/R_c = 0.8, AND υ = 0.0025. THE REAL OSCILLATION FREQUENCY IS OBTAINED FOR Δ = 0.

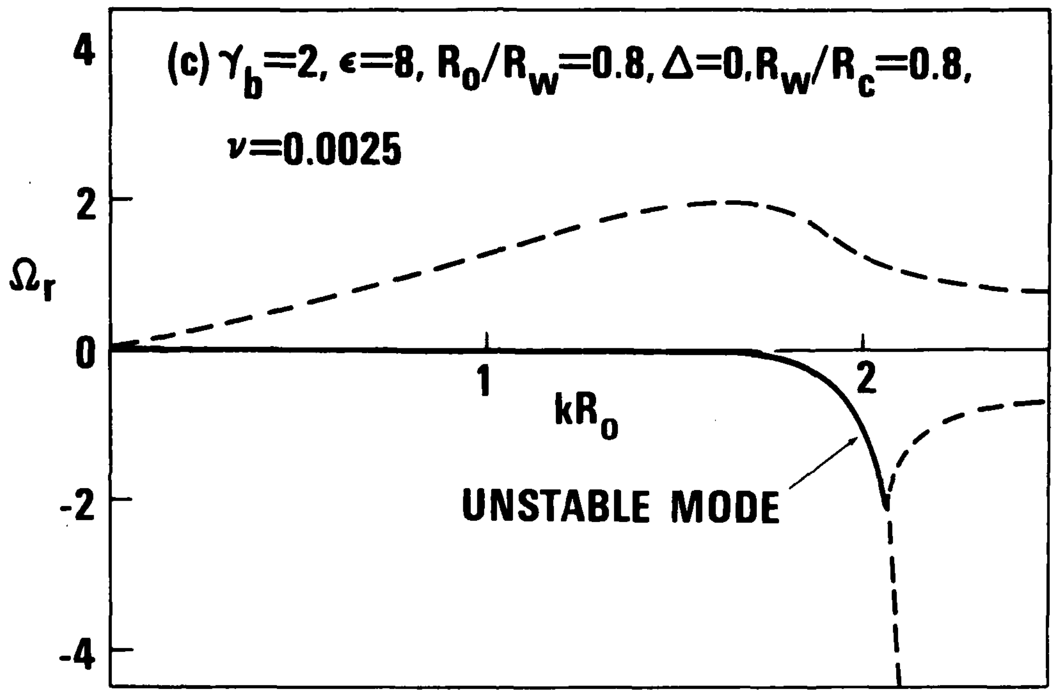

FIGURE 13c PLOTS OF DOPPLER-SHIFTED REAL OSCILLATION FREQUENCY Ω_r = ReΩ VERSUS kR_0 [EQS. (57), (58), AND (61)] FOR γ_b = 2, ϵ = 8, R_0/R_w = 0.8, R_w/R_c = 0.8, AND υ = 0.0025. THE REAL OSCILLATION FREQUENCY IS OBTAINED FOR Δ = 0.

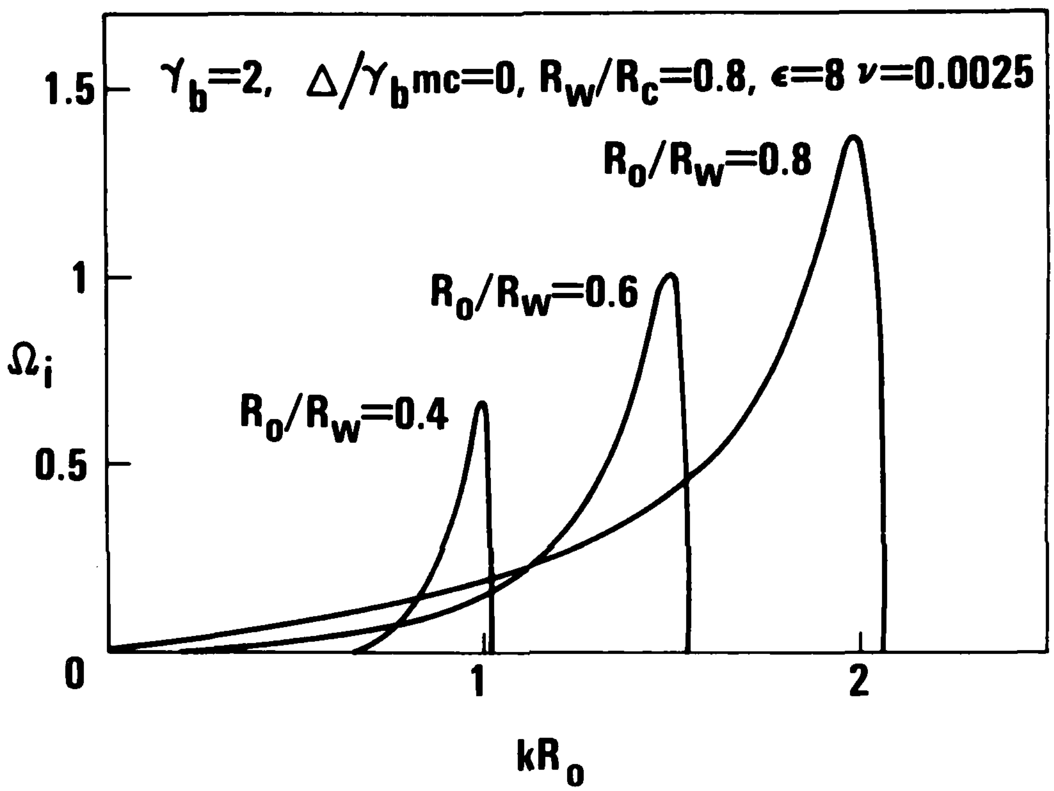

FIGURE 14 PLOT OF THE NORMALIZED GROWTH RATE Ω_i = 1mΩ VERSUS kR_0 [EQ. (61)] FOR Δ = 0, SEVERAL VALUES OF R_0/R_w, AND PARAMETERS OTHERWISE IDENTICAL TO FIGURE 13.

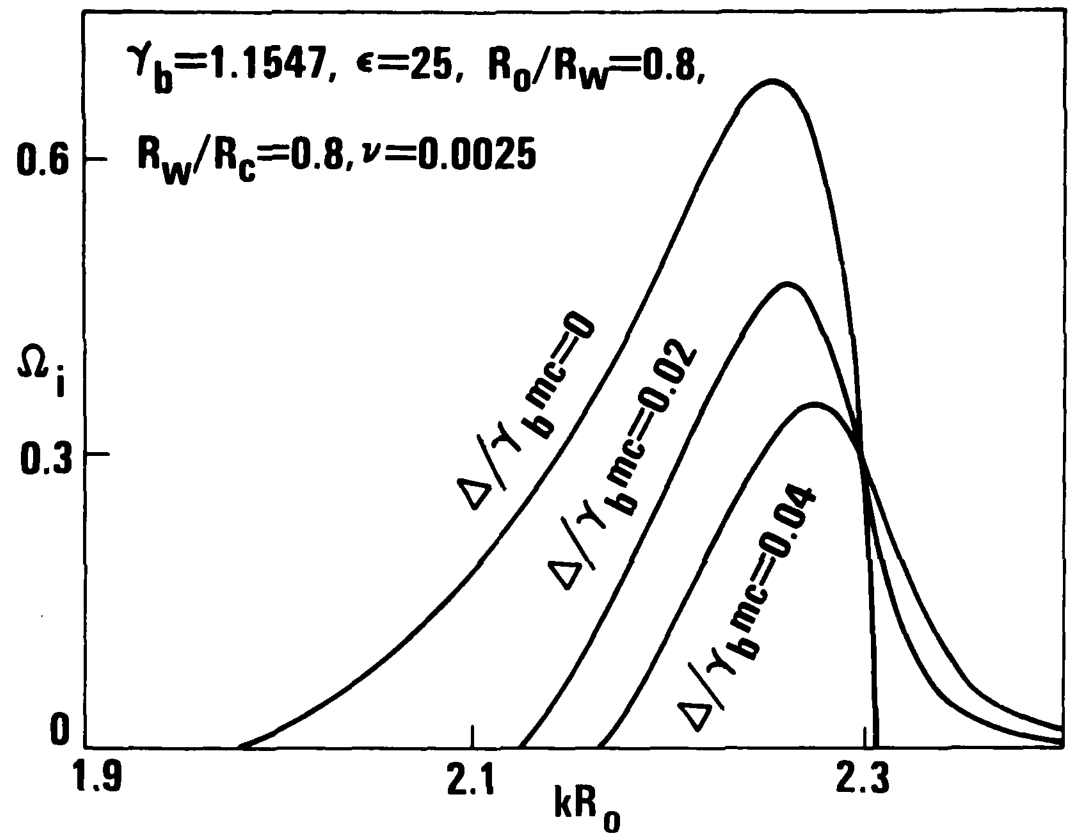

FIGURE 15 PLOT OF THE NORMALIZED GROWTH RATE VERSUS kR_0 [EQ. (61)] FOR γ_b = 1.1547, ϵ = 25, AND PARAMETERS OTHERWISE IDENTICAL TO FIGURE 13.

REFERENCES

1. R. C. Davidson, Theory of Nonneutral Plasmas, (Benjamin, Reading, Mass., 1974), Ch. 2.
2. H. S. Uhm and M. Lampe, "Stability Properties of Azimuthally Symmetric Perturbations in an Intense Electron Beam", submitted for publication.
3. R. J. Briggs, Phys. Fluids 19, 1257 (1976).
4. P. Sprangle, A. T. Drobot, and W. M. Manheimer, Phys. Rev. Lett. 36, 1180 (1976).
5. C. W. Roberson and F. Mako, Bull. Am. Phys. Soc. 25, 1008 (1980).
6. V. Serlin, R. J. Adler, J. A. Nation, G. Providakes, Bull. Am. Phys. Soc. 25, 1008 (1980).
7. R. C. Davidson and H. S. Uhm, Phys. Fluids 23, 2076 (1980).
8. H. S. Uhm and R. C. Davidson, "Free Electron Laser Instability for a Solid Relativistic Electron Beam", submitted for publication.
9. J. Walch, D. Kapilow, R. Layman, D. Speer, J. Branscum, D. Wise, and C. Hanna, Bull. Am. Phys. Soc. 25, 949 (1980).
10. C. K. Birdsall and J. P. Whinnery, J. Appl. Phys. 24, 314 (1953).
11. J. D. Jackson, Classical Electrodynamics, (John Wiley & Sons, Inc., New York, 1962), Ch. 14.
12. H. S. Uhm and R. C. Davidson, Phys. Fluids 23, 1586 (1980).

DISTRIBUTION

	Copies
Naval Research Laboratory Attn: Dr. M. Lampe Washington, D. C. 20365	1
Office of Naval Research Attn: W. J. Condell (ONR-421) Washington, D. C. 20350	1
U. S. Army Ballistic Research Laboratory Aberdeen Proving Ground Attn: Dr. D. Eccleshall (DRDAR-BLB) Aberdeen, Maryland 21005	1
Air Force Weapons Laboratory Kirtland Air Force Base Attn: Maj. H. Dogliana Albuquerque, New Mexico 87117	1
Department of Energy Attn: Dr. T. Godlove (C-404) Washington, D. C. 20545	1
National Bureau of Standards Attn: Dr. J. M. Leiss Gaithersburg, Maryland 20760	1
Austin Research Associates, Inc. Attn: Dr. W. E. Drummond 1901 Rutland Drive Austin, Texas 78758	1
Ballistic Missile Defense Advanced Technology Center Attn: Dr. L. J. Harvard (BMDSATC-1) P. O. Box 1500 Huntsville, Alabama 35807	1
B. K. Dynamics, Inc. Attn: Dr. R. Linz 15825 Shady Grove Road Rockville, Maryland 20850	1

DISTRIBUTION (con't.)

	Copies
The Charles Stark Draper Laboratory, Inc. Attn: Dr. E. Olsson 555 Technology Square Cambridge, Massachusetts 02139	1
Director Defense Advance Research Projects Agency Attn: Dr. J. Mangano 1400 Wilson Boulevard Arlington, Virginia 22209	1
IRT Corporation Attn: Mr. W. Selph P.O. Box 81087 San Diego, California 92138	1
Los Alamos Scientific Laboratory Attn: Dr. G. Best P.O. Box 1663 Los Alamos, New Mexico 87545	1
Mission Research Corporation Attn: Dr. C. Longmire 735 State Street Santa Barbara, California 93102	1
Physical Dynamics, Inc. Attn: Dr. K. Breuckner P.O. Box 977 La Jolla, California 92037	1
Sandia Laboratories Attn: Mail Services Section for: Dr. R.B. Miller Albuquerque, New Mexico 87115	1
Science Applications, Inc. Attn: Dr. M.P. Fricke 1200 Prospect Street La Jolla, California 92037	1

DISTRIBUTION (con't.)

	Copies
Science Applications, Inc.	
Attn: Dr. R. Johnston	1
Dr. J. Siambis	1
2680 Hanover Street	
Palo Alto, California 94304	
University of California	
Lawrence Livermore Laboratory	
Attn: Dr. R.J. Briggs	1
Dr. E. Lee	1
P.O. Box 808	
Livermore, California 94550	
Defense Technical Information Center	
Cameron Station	12
Alexandria, Virginia 22314	
Naval Sea Systems Command	
Washington, D.C. 20362	
Attn: SEA-09G32	2
SEA-03B	1

NDW-NSWC(W)-5605/1 (Rev. 5-78)

TO AID IN UPDATING THE DISTRIBUTION LIST FOR NAVAL SURFACE WEAPONS CENTER, WHITE OAK TECHNICAL REPORTS PLEASE COMPLETE THE FORM BELOW:

TO ALL HOLDERS OF NSWC/TR 81-65
by Han S. Uhm, Code R41

DO NOT RETURN THIS FORM IF ALL INFORMATION IS CURRENT

A. FACILITY NAME AND ADDRESS *(OLD) (Show Zip Code)*

NEW ADDRESS *(Show Zip Code)*

B. ATTENTION LINE ADDRESSES:

C.

☐ REMOVE THIS FACILITY FROM THE DISTRIBUTION LIST FOR TECHNICAL REPORTS ON THIS SUBJECT.

D.

NUMBER OF COPIES DESIRED ______________________

GPO 930-784

DEPARTMENT OF THE NAVY
NAVAL SURFACE WEAPONS CENTER
WHITE OAK, SILVER SPRING, MD. 20910

OFFICIAL BUSINESS
PENALTY FOR PRIVATE USE, $300

POSTAGE AND FEES PAID
DEPARTMENT OF THE NAVY
DOD 316

COMMANDER
NAVAL SURFACE WEAPONS CENTER
WHITE OAK, SILVER SPRING, MARYLAND 20910

ATTENTION: CODE R41